

Chiral Solitons in the Spectral Quark Model

Enrique Ruiz Arriola*

*Departamento de Física Atómica, Molecular y Nuclear,
Universidad de Granada, E-18071 Granada, Spain*

Wojciech Broniowski†

*The H. Niewodniczański Institute of Nuclear Physics, PL-31342 Kraków, Poland and
Institute of Physics, Świętokrzyska Academy, ul. Świętokrzyska 15, PL-25406 Kielce, Poland*

Bojan Golli‡

*Faculty of Education, University of Ljubljana, 1000 Ljubljana, Slovenia and
J. Stefan Institute, 1000 Ljubljana, Slovenia*

(Dated: August 29, 2018)

Chiral solitons with baryon number one are investigated in the Spectral Quark Model. In this model the quark propagator is a superposition of complex-mass propagators weighted with a suitable spectral function. This technique is a method of regularizing the effective quark theory in a way preserving many desired features crucial in analysis of solitons. We review the model in the vacuum sector, stressing the feature of the absence of poles in the quark propagator. We also investigate in detail the analytic structure of meson two-point functions. We provide an appropriate prescription for constructing valence states in the spectral approach. The valence state in the baryonic soliton is identified with a saddle point of the Dirac eigenvalue treated as a function of the spectral mass. Due to this feature the valence quarks never become unbound nor dive into the negative spectrum, hence providing stable solitons as absolute minima of the action. This is a manifestation of the absence of poles in the quark propagator. Self-consistent mean field hedgehog solutions are found numerically and some of their properties are determined and compared to previous chiral soliton models. Our analysis constitutes an involved example of a treatment of a relativistic complex-mass system.

PACS numbers: 12.38.Lg, 11.30, 12.38.-t

Keywords: chiral quark models, baryon, soliton

I. INTRODUCTION

The original proposal by Skyrme of the early sixties foresaw that baryons could be described as classical topological solitons of a specific non-linear chirally symmetric Lagrangean in terms of meson fields with non-trivial boundary conditions [1]. Within the accepted QCD framework the large- N_c analysis under the assumption of confinement [2, 3] supports many aspects of this view. Moreover, the identification of the topological winding number as the conserved baryon number of quarks from the occupied Dirac sea in the background of large and spatially extended pion fields [4] suggested the underlying necessary fermionic nature of the soliton at least for odd N_c [5]. The form of the Lagrangean remains unspecified besides the requirement of chiral symmetry, leaving much freedom on the assumed meson-field dynamics needed for practical computations of low-energy baryonic properties [6, 7], usually organized in terms of a finite number of bosons of increasing mass. One appealing feature of the Skyrme model (for reviews see e.g. [8, 9, 10, 11]) is that confinement appears to be explicitly

incorporated, since the baryon number topology of the meson fields cannot be changed with a finite amount of energy and the soliton is absolutely stable against decay into free quarks. This has also made possible the study of excited baryons (see e.g. Ref. [12] and references therein). However, when the partonic content of the baryon is analyzed in deep inelastic scattering, in the Skyrme model the Callan-Gross relation is violated, hence the partons turn out not to be spin one-half objects [13]. Therefore, making credible non-perturbative estimates of high energy properties is out of reach of the standard Skyrme model. This also suggests that the relevant degrees of freedom should explicitly include constituent quarks chirally coupled to mesons [14, 15, 16, 17, 18, 19, 20, 21, 22] motivating the use of chiral quark models with quarks and to search for solitonic solutions to describe baryons. The approach is very much in the spirit of the Skyrme model but with the important feature that the partonic interpretation corresponds to spin one-half constituents, despite the subtleties of the regularization [23]. The considerable effort exerted to describe low-lying baryons as solitons of effective chiral quark models has been described in detail in the reviews [24, 25, 26, 27, 28].

The chiral quark models that arise naturally in several approaches to low-energy quark dynamics, such as the instanton-liquid model [29] or the Schwinger-Dyson resummation of rainbow diagrams [30], are *nonlocal*, i.e. the quark mass function depends on the quark virtual-

*Electronic address: earriola@ugr.es

†Electronic address: Wojciech.Broniowski@ifj.edu.pl

‡Electronic address: bojan.golli@ijs.si

ity. For the derivations and applications of these models see, *e.g.*, [31, 32, 33, 34, 35, 36, 37, 38, 39, 40, 41, 42, 43, 44, 45, 46, 47]. A major success was the finding of baryon hedgehog solitons in nonlocal models [48, 49], which turn out to be stable also in the linear version of the model. Moreover, the nonlocal models have nice features as compared to the local variants, in particular they use a uniform regularization of both the normal and abnormal parity processes, thus reproducing properly the anomalies in the presence of regularization. In addition, the theory is made finite to all orders of perturbation theory. The price to pay for the non-locality is a complicated nature of interaction vertices with currents, where the gauge invariance imposes non-local contributions. Their presence leads to technical complications in the treatment of non-local models.

A relevant issue for chiral quark solitons is related to the confinement and stability of the mean field solution. The chiral quark soliton model builds baryons as bound states of valence constituent quarks in non-trivial meson fields. Indeed, such a model interpolates between the non-relativistic quark model and the Skyrme model in the limit of small solitons and large solitons, respectively [50]. As a matter of fact, from the view point of the chiral quark model, the apparent confinement in the Skyrme model is reinterpreted as a strong binding effect, and indeed deeply bound states are not sensitive to the confinement properties of the interaction. Nevertheless, it is notorious that depending on the details, the mean field soliton may in fact decay into three free constituent quarks. Moreover, in local models for small enough solitons the valence state becomes an unbound free quark at rest. Actually, to our knowledge there is no satisfactory calculation of excited baryon states in the chiral quark soliton model precisely because of the lack of confinement [51]. These features happen for realistic parameter values and despite the alleged compatibility of the chiral quark model with the large- N_c limit. As already mentioned the soliton description of baryons in the large- N_c limit is based on the assumption of confinement.

Let us define the scope of the present work. After the many years, the issue of color confinement remains a crucial and intriguing subject for which no obvious solution exists yet. In particular, its realization implies two relevant consequences. In the first place, there exists a spectrum of color singlet excited states. Secondly, quarks cannot become on shell and hence quark propagators merely cannot have poles on the real axis. This restrained meaning of confinement is often called *analytic confinement* in the literature and in that sense is adopted in the present work. We hasten to emphasize that although our work obviously *does not* suggest how the problem of color confinement might be resolved, we manage to set up a framework where the calculation of color singlet states such as excited baryons becomes possible as a matter of principle within a chiral quark soliton approach.

In this paper we show how a recently proposed ver-

sion of the chiral quark model, the Spectral Quark Model (SQM) [52, 53, 54, 55] (see also [56] for the original insights on the spectral problem), not only allows for solitonic solutions but due to its unconventional and indeed remarkable analytic properties yields a valence eigenvalue which never becomes unbound. Thus the soliton is absolutely stable. The model is based on a generalized Lehmann representation where the spectral function is generically complex, involving a continuous superposition of complex masses. The subject of defining a well founded quantum field theory of fixed complex masses is an old story [57, 58, 59, 60, 61]. Our approach differs from these works, since our complex mass is an integration variable so that many standard objections are sidestepped by choosing an appropriate integration contour. In practical terms the spectral function acts as a finite regulator fulfilling suitable spectral conditions but with many desirable properties, in particular the simple implementation of chiral symmetry and gauge invariance. One of its outstanding features is the uniform treatment of normal and abnormal parity processes ensuring both finiteness of the action and a simultaneous implementation of the correctly normalized Wess-Zumino-Witten term¹. This uniform treatment of regularization has some impact on soliton calculations even in the SU(2) case (where the Wess-Zumino-Witten term vanishes) since the valence and sea contributions to the soliton energy are indeed related to the abnormal and normal parity separation of the effective action, respectively. The basics of SQM are described in detail in [53, 55] and the reader is referred there for the description of the method and numerous applications to the pion phenomenology. The SQM approach bares similarities to nonlocal models, however the construction of interaction vertices with currents is very simple in SQM, as opposed to almost prohibitive complications of the nonlocal approach.

The purpose of this paper is twofold: Firstly, we show that absolutely stable baryon solitons in SQM exist and discuss their properties. Secondly and more generally, we study an instance of an involved complex-mass system, and show how to treat valence states. Despite the complexity, the resulting prescription turns out to be very simple and easy to implement in practical calculations. It amounts to locating the saddles of the valence eigenvalue, ϵ_0 , as a function of the complex mass ω , based on the condition

$$\frac{d\epsilon_0(\omega)}{d\omega} = 0. \quad (1)$$

The outline of our paper is as follows: In Sect. II we provide an operational justification of the need of some

¹ In the standard treatment of local models the somewhat artificial and certainly asymmetric prescription of regularizing the real part of the Euclidean action and not regularizing the imaginary part has been used.

uniform regularization for the full action without an explicit separation between normal and abnormal parity contributions. Certain *a priori* field-theoretic consistency conditions are discussed. SQM is shown to fulfill the *one-body* consistency condition in contrast to previous local versions of chiral quark models. We also discuss in some detail the analytic structure of the meson correlators, showing that despite analytically-confined quarks they possess cuts at large values of q^2 , as requested by (asymptotic) quark unitarity. However, the meromorphic structure expected from general large N_c considerations is violated. This point is analyzed in the light of a large- N_c Regge model. Next, we pass to the analysis of solitons. First, we discuss the connection between the baryon and topological currents in the limit of large solitons, which holds in the presence of the spectral regularization. Following the standard field-theoretic approach the construction of the baryon state is pursued in Sect. III. The unconventional appearance of complex-masses requires a demanding mathematical treatment of both the valence and sea contributions. Nevertheless, ready-to-use formulas for the total soliton mass are derived and analyzed for several soliton profiles showing the existence of chiral solitons with baryon number one. An alternative derivation is provided in Appendix E based on computing the spectral integral exactly. Dealing with complex mass Dirac operators both for bound states and continuum states is involved and some of the features may be studied in a somewhat comprehensive toy model in Appendix D. The techniques are close to the more familiar complex potentials in non-relativistic quantum mechanics which are reviewed for completeness in Appendix C. In Appendix G we show that a linear extension of SQM leads to instability of the vacuum, hence SQM can only be constructed in the originally proposed non-linear realization. In Sect. IV we look for self-consistent hedgehog solutions and determine their properties both in the chiral limit as well as for finite pion masses. Finally, in Sect. V we come to the conclusions.

II. THE SPECTRAL QUARK MODEL AND CONSISTENCY RELATIONS

We begin with some basic expressions of the general field-theoretic treatment of chiral quark models, which are the groundwork for our treatment of solitons and the method of including valence states in SQM discussed in Sect. III. In this section we highlight an important consistency condition which was not fulfilled in the hitherto extensively used chiral quark soliton models based on local interactions. Remarkably, this condition happens to be satisfied in SQM. The analytic properties of the quark propagator and in particular the lack of poles are reviewed. We also analyze some important aspects of the meson sector, and in particular the analytic structure of two-point correlators in the complex q^2 -plane. Finally, we show how the correct topological current arises in the

presence of regularization.

A. A consistency condition

The vacuum-to-vacuum transition amplitude in the presence of *external* bosonic (s, p, v, a) and fermionic ($\eta, \bar{\eta}$) fields of a chiral quark model Lagrangian can be written in the path-integral form as

$$Z[j, \eta, \bar{\eta}] = \langle 0 | T \exp \left\{ i \int d^4x \left[\bar{q} j q + \bar{\eta} q + \bar{q} \eta \right] \right\} | 0 \rangle, \quad (2)$$

where the compact notation

$$j = \not{p} + \not{a} \gamma_5 - (s + i \gamma_5 p) \quad (3)$$

has been introduced. The symbols s, p, v_μ , and a_μ denote the external scalar, pseudoscalar, vector, and axial flavor sources, respectively, given in terms of the generators of the flavor $SU(3)$ group,

$$s = \sum_{a=0}^{N_F^2-1} s_a \frac{\lambda_a}{2}, \quad \dots \quad (4)$$

with λ_a representing the Gell-Mann matrices. Any physical matrix element can be computed by functional differentiation with respect to the external sources.

Let us consider the calculation of a bilinear quark operator, such as, *e.g.*, the quark condensate (for a single flavor) $\langle \bar{q} q \rangle$. We can think of two possible ways of making such a computation, namely via coupling of an external scalar source $s(x)$ (a mass term) and differentiating with respect to $s(x)$, or by calculating the second functional derivative with respect to the Grassmann external sources $\eta(x)$ and $\bar{\eta}(x)$ taken at the same spatial point. The consistency of the calculation requires the following trivial identity for the generating functional:

$$\begin{aligned} \langle \bar{q}(x) q(x) \rangle &= i \frac{1}{Z} \frac{\delta Z}{\delta s(x)} \Big|_0 \\ &= \lim_{x' \rightarrow x} \langle \bar{q}(x') q(x) \rangle = \lim_{x' \rightarrow x} (-i)^2 \frac{1}{Z} \frac{\delta^2 Z}{\delta \eta(x) \delta \bar{\eta}(x')} \Big|_0, \quad (5) \end{aligned}$$

where $|_0$ means all external sources set to zero. This requirement can be generalized to any quark bilinear with any bosonic quantum numbers and thus we call it the *one-body consistency condition*. In the traditional treatment of local chiral quark models the l.h.s. of the above formula corresponds to a closed quark line and is divergent, calling for regularization, whereas for $x' \neq x$ the r.h.s. is finite and corresponds to an open quark line, thus no regularization is demanded. This poses a consistency problem which actually becomes crucial in the analysis of high-energy processes and introduces an ambiguity in the partonic interpretation as well as conflicts with gauge invariance and energy-momentum conservation (see, *e.g.*, Ref. [62] for a further discussion on these subtle but relevant issues). Obviously, the previous argument could

equally be applied to sources with any quantum numbers suggesting that any *consistent* regularization should be applied to the full action. As already mentioned in the Introduction, in the traditional approach to local models the treatment of singularities requires first to separate the normal and abnormal parity contributions and to regularize only the normal parity piece. In the Euclidean space this separation corresponds to the real and imaginary parts of the action.

In the next section we show that SQM fulfills the one-body consistency condition. More generally, one might want to extend the condition (5) to any number of quark bilinears contracted to bosonic quantum numbers, namely the N -body consistency condition

$$\begin{aligned} & \langle \bar{q}(x_1)\Gamma_1 q(x_1) \cdots \bar{q}(x_N)\Gamma_N q(x_N) \rangle \\ &= \lim_{x'_i \rightarrow x_i} \langle \bar{q}(x'_1)\Gamma_1 q(x_1) \cdots \bar{q}(x'_N)\Gamma_N q(x_N) \rangle \end{aligned} \quad (6)$$

where the l.h.s. is evaluated after functional derivatives with respect to bosonic sources and the r.h.s. with respect to fermionic sources respectively. Here Γ_i are general spin-flavor matrices. We have found that this is not possible in the SQM scheme (see the discussion in Sect. II B below).

B. The Spectral Quark Model and the quark propagator

In SQM the regularization is imposed already at the level of one open line through the use of a generalized Lehmann representation for the full quark propagator in the absence of external sources,

$$S(\not{p}) = \int_C d\omega \frac{\rho(\omega)}{\not{p} - \omega} = \not{p}A(p^2) + B(p^2) \quad (7)$$

where C is a suitable contour in the complex mass-plane [54] (see also Fig. 1 below). Chiral and electromagnetic gauge invariance can be taken care of through the use of the gauge technique of Delbourgo and West [63, 64], which provide particular solutions to chiral Ward-Takahashi identities, or through the use of the standard effective action approach, applied in this paper. As a result, one can “open the quark line” from one closed loop and compute high-energy processes with a partonic interpretation, such as, *e.g.*, the structure function and the light-cone wave function of the pion, *etc.* [54], or the photon and ρ -meson light cone wave functions [65]. The generalization of the (one body) consistency condition for scalar sources, Eq. (5), to all possible bosonic quantum numbers can be achieved by taking the generating functional to be

$$Z[\eta, \bar{\eta}, s, p, v, \dots] = \int D U e^{-i\langle \bar{\eta}, S[U, s, p, v, a] \eta \rangle} e^{i\Gamma[U, s, p, v, a]}, \quad (8)$$

where the quark propagator and the effective action are given by

$$\langle x' | S[U, s, p, v, a]_{aa'} | x \rangle = \int_C d\omega \rho(\omega) \langle x | (\mathbf{D})_{aa'}^{-1} | x' \rangle, \quad (9)$$

and

$$\Gamma[U, s, p, v, a] = -iN_c \int_C d\omega \rho(\omega) \text{Tr} \log(i\mathbf{D}), \quad (10)$$

respectively. The Dirac operator has the form

$$i\mathbf{D} = i\not{\partial} - \omega U^5 - \hat{m}_0 + (\not{p} + \not{a}\gamma_5 - s - i\gamma^5 \not{p}).$$

For a bilocal (Dirac- and flavor-matrix valued) operator $A(x, x')$ we use the notation

$$\text{Tr} A = \int d^4x \text{tr} \langle A(x, x) \rangle, \quad (11)$$

with tr denoting the Dirac trace and $\langle \rangle$ the flavor trace. The matrix

$$\begin{aligned} U^5 &= e^{i\gamma_5 \sqrt{2}\Phi/f} \\ &= \frac{1}{2}(1 + \gamma_5)U + \frac{1}{2}(1 - \gamma_5)U^\dagger, \end{aligned} \quad (12)$$

while $U = u^2 = e^{i\sqrt{2}\Phi/f}$ is the flavor matrix representing the pseudoscalar octet of mesons in the nonlinear representation,

$$\Phi = \begin{pmatrix} \frac{1}{\sqrt{2}}\pi^0 + \frac{1}{\sqrt{6}}\eta & \pi^+ & K^+ \\ \pi^- & -\frac{1}{\sqrt{2}}\pi^0 + \frac{1}{\sqrt{6}}\eta & K^0 \\ K^- & \bar{K}^0 & -\frac{2}{\sqrt{6}}\eta \end{pmatrix}. \quad (13)$$

The matrix $\hat{m}_0 = \text{diag}(m_u, m_d, m_s)$ is the current quark mass matrix and $f = 86$ MeV denotes the pion weak-decay constant in the chiral limit, ensuring the proper normalization condition of the pseudoscalar fields. For a two-flavor model it is enough to consider $\Phi = \vec{\tau} \cdot \vec{\pi}/\sqrt{2}$.

In Eq. (8) the Dirac operator appears both in the fermion determinant as well as in the quark propagator and could, in principle, be treated independently. The one-body consistency condition is fulfilled *precisely* because we use the same spectral function $\rho(\omega)$ for both. We have refrained on purpose from writing a Lagrangean in terms of quarks explicitly since anyhow chiral quark models are defined in conjunction with the regularization and the approximation used. In our case we work in the leading order of the large- N_c expansion, which amounts to a saddle point approximation in the bosonic U -fields and use the spectral regularization which is most explicitly displayed in terms of the generating functional presented above. The new ingredient of SQM compared to earlier chiral quark models is the presence of the quark spectral function $\rho(\omega)$ in Eq. (9,10) and the integration over ω along a suitably chosen contour C in the complex- ω plane. Our approach extends the early model of Efimov and Ivanov [56] by including the gauge invariance, the chiral symmetry, and the vector meson dominance, as well as applying the model to both low- and high-energy processes.

The above SQM construction implements the one-body consistency condition, as follows

$$i \frac{\delta Z}{\delta \bar{j}_\alpha(x)} \Big|_{\eta=\bar{\eta}=0} = \lim_{x' \rightarrow x} (-i)^2 \frac{\delta}{\delta \eta(x)} \Gamma_\alpha \frac{\delta}{\delta \bar{\eta}(x')} Z \Big|_{\eta=\bar{\eta}=0}, \quad (14)$$

which is more general than Eq. (5) since it is valid in the presence of non-vanishing external bosonic sources with any quantum numbers and non-trivial background pion field, U . This represents a clear improvement on the previous *local* chiral quark models where this requirement was violated. Eq. (14) has direct applicability on the soliton sector as we will discuss in Sect. III. It should be mentioned, however, that similarly to many other chiral quark models, the two-body and higher consistency conditions, Eq. (6) are not satisfied in SQM. For instance, for the two body consistency condition one gets

$$\begin{aligned} \langle \bar{q}(x_1) \Gamma_1 q(x_1) \bar{q}(x_2) \Gamma_2 q(x_2) \rangle &= \frac{1}{Z} \int DU \int d\omega \rho(\omega) \\ &\times \text{tr} [\Gamma_1 \langle x_1 | \mathbf{D}^{-1}(\omega) | x_1 \rangle] \text{tr} [\Gamma_2 \langle x_2 | \mathbf{D}^{-1}(\omega) | x_2 \rangle], \end{aligned} \quad (15)$$

while

$$\begin{aligned} \lim_{x'_i \rightarrow x_i} \langle \bar{q}(x_1) \Gamma_1 q(x'_1) \bar{q}(x_2) \Gamma_2 q(x'_2) \rangle &= \lim_{x'_i \rightarrow x_i} \frac{1}{Z} \int DU \\ &\times \int d\omega_1 \rho(\omega_1) \text{tr} [\Gamma_1 \langle x'_1 | \mathbf{D}^{-1}(\omega_1) | x_1 \rangle] \\ &\times \int d\omega_2 \rho(\omega_2) \text{tr} [\Gamma_2 \langle x'_2 | \mathbf{D}^{-1}(\omega_2) | x_2 \rangle] \\ &\neq \langle \bar{q}(x_1) \Gamma_1 q(x_1) \bar{q}(x_2) \Gamma_2 q(x_2) \rangle. \end{aligned} \quad (16)$$

Likewise, we do not know if this one body consistency condition is fulfilled beyond the leading large- N_c approximation. At present the only known way to fulfill all consistency conditions is by returning to nonlocal versions of the chiral quark model. Therefore, we must provide a prescription of how higher functional derivatives should be handled in case were more than a single quark line could be opened. Eq. (14) suggests to use *always* the method based on the bosonic sources for operators involving any number of quark bilinear and local operators. For operators involving one single bilocal and bilinear operator $q(x) \bar{q}(x')$ we may use the method based on fermionic sources, since Eq. (14) guarantees the consistency in the coincidence limit $x' \rightarrow x$. Of course, this prescription does not yield a unique result when more than one bilocal and bilinear quark operator is involved or equivalently when more than one quark line is opened.

Using the standard variational differentiation for the generating functional the Feynman rules for SQM follow from the action (10). They have the form of the usual Feynman rules for a local theory, amended with the spectral integration associated to each quark line, according to Eq. (10). This resembles very much the well known Pauli-Villars regularization method (however with a continuous superposition of complex masses) and allows for very efficient computations, see [52, 53, 54, 55].

The basic paper [53] explains the general construction and the conditions for the moments of the spectral function $\rho(\omega)$ coming from physics constraints. In particular, normalization requires

$$\int_C d\omega \rho(\omega) = 1, \quad (17)$$

while observables are related to the log-moments and inverse moments of $\rho(\omega)$ [53]. The full spectral function consists of two parts of different parity under the change $\omega \rightarrow -\omega$, *i.e.* $\rho(\omega) = \rho_V(\omega) + \rho_S(\omega)$, with the scalar part, ρ_S , even and the vector part, ρ_V , odd. A particular implementation of SQM is the *meson dominance model*, where one requests that the large- N_c pion electromagnetic form factor has the monopole form of the vector-meson dominance (VMD),

$$F_\pi(q^2) = \frac{M_V^2}{M_V^2 - q^2}, \quad (18)$$

where M_V denotes the ρ -meson mass.² The matching of the model predictions to this form yields the rather unusual spectral function

$$\rho_V(\omega) = \frac{1}{2\pi i} \frac{1}{\omega} \frac{1}{(1 - 4\omega^2/M_V^2)^{5/2}}, \quad (19)$$

with the pole at the origin and cuts starting at $\pm M_V/2$, where M_V is the mass of the vector meson. Similar considerations for the photon light-cone wave function [65] and matching to VMD yield for the scalar part an analogous form,

$$\rho_S(\omega) = -\frac{1}{2\pi i} \frac{48\pi^2 \langle \bar{q}q \rangle}{N_c M_S^4 (1 - 4\omega^2/M_S^2)^{5/2}}. \quad (20)$$

where $\langle \bar{q}q \rangle$ is the single flavor quark condensate, and $M_S = M_V$ [55]. The contour C for the ω integration to be used with formulas (19,20) is shown in Fig. 1 for ρ_V (for ρ_S one has the same contour with $M_V \rightarrow M_S$). This contour is applicable in the vacuum (*i.e.*, no baryon number) sector of the model. The extension to baryons is described in the next section. From Eq. (19) and (20) one gets the quark propagator functions from Eq. (7),

$$\begin{aligned} A(p^2) &= \int_C d\omega \frac{\rho_V(\omega)}{p^2 - \omega^2} \\ &= \frac{1}{p^2} \left[1 - \frac{1}{(1 - 4p^2/M_V^2)^{5/2}} \right], \\ B(p^2) &= \int_C d\omega \frac{\omega \rho_S(\omega)}{p^2 - \omega^2} \\ &= \frac{48\pi^2 \langle \bar{q}q \rangle}{M_S^4 N_c (1 - 4p^2/M_S^2)^{5/2}}. \end{aligned} \quad (21)$$

These functions do not possess poles (the alleged pole at $p^2 = 0$ in $A(p^2)$ is canceled), but only cuts starting at

² This example shows in a transparent way a peculiar feature of the model. In the standard constant mass case the pion form factor, a three point function, due to Cutkosky's rules, displays a cut in the form factor for sufficiently large energy due to a superposition of poles in the quark propagator. In SQM the mechanism is just the opposite; the cuts conspire to build a pole in the form factor.

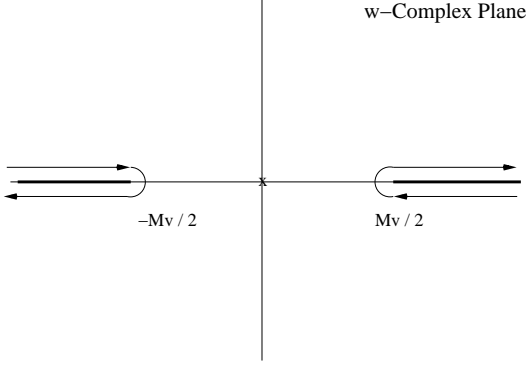


FIG. 1: The contour C in the complex- ω plane for the calculations in the vacuum sector in the meson dominance variant of SQM. M_V denotes the ρ -meson mass. The two segments shown in the figure are connected at \pm infinity with semi-circles, not displayed.

$p^2 = M_V^2/4$, reflecting the structure of $\rho(\omega)$. Actually, the ω -integral can be evaluated using the integral transformations displayed in the first lines of Eqs. (21). For instance, taking the limit $p^2 \rightarrow \infty$ one gets the moments

$$\delta_{k,0} = \int_C d\omega \rho_V(\omega) \omega^{2k}, \quad k = 0, 1, 2, \dots \quad (22)$$

$$0 = \int_C d\omega \rho_S(\omega) \omega^{2k+1}, \quad k = 0, 1, 2, \dots \quad (23)$$

which imply in particular the vanishing of all positive moments for the spectral function $\rho(\omega)$.

The pion weak-decay constant in the chiral limit comes out to be [53]

$$f^2 = \frac{N_c M_V^2}{24\pi^2}, \quad (24)$$

a relation which works well phenomenologically. This relation will be used as an identity in the rest of the paper. Compared to the standard field-theoretic case, each quark line is supplemented with a spectral integration $\int_C d\omega \rho(\omega)$. This makes calculations very straightforward and practical for numerous hadronic processes involving mesons and photons. We stress that despite a rather “exotic” appearance of the quark spectral function, SQM leads to proper phenomenology for the soft pion, including the Gasser-Leutwyler coefficients [55], the soft matrix elements for hard processes, such as the distribution amplitude, transition form factor, or structure functions [53], the generalized forward parton distribution of the pion [67], the photon distribution amplitude and light-cone wave functions [65], or the pion-photon transition distribution amplitude [66]. In addition, the calculations are straightforward, leading to simple analytic results. Interestingly, the quark propagator corresponding to (19,20) has no poles, only cuts, in the momentum space. The evaluated mass function of the quark, $M(Q^2)$, displays a typical dependence on the virtuality Q^2 in the Euclidean region and at the qualitative

and quantitative level compares favorably to the non-local quark models and to the lattice calculations [68]. As a sample calculation, we extend in the next subsections the previous considerations to the calculation of vacuum properties and two-point correlators.

C. The vacuum sector

As mentioned above the functional (one-body) consistency conditions guarantee the unambiguous calculation of observables obtained from quark fields, either as double Grassmann functional derivatives or as single bosonic ones. These identities are generically formally satisfied but become tricky under regularization. Here we use the first possibility for the quark condensate and the vacuum energy density. The second method based on the effective action and yielding identical results is outlined in Appendix A.

The (single flavor) quark condensate $\langle \bar{q}q \rangle$ can directly be computed from the quark propagator

$$\begin{aligned} N_f \langle \bar{q}q \rangle &= -iN_c \int \frac{d^4 p}{(2\pi)^4} \text{Tr} S(p) \\ &= 4N_c N_f \frac{1}{i} \int \frac{d^4 p}{(2\pi)^4} B(p^2), \end{aligned} \quad (25)$$

which through the use of Eq. (21) becomes an identity. The vacuum energy density can be computed by using the trace of the energy momentum tensor, yielding

$$\begin{aligned} \langle \theta^{\mu\nu} \rangle &= \langle \bar{q}(x) \frac{i}{4} [\gamma^\nu \overleftrightarrow{\partial}^\mu + \gamma^\mu \overleftrightarrow{\partial}^\nu] q(x) \rangle \\ &= -iN_c \int \frac{d^4 p}{(2\pi)^4} \text{Tr} \left[\frac{1}{2} (p^\mu \gamma^\nu + p^\nu \gamma^\mu) S(p) \right] \\ &= -4iN_c N_f \int \frac{d^4 p}{(2\pi)^4} p^\mu p^\nu A(p^2) \\ &= \frac{1}{4} g^{\mu\nu} \epsilon + \langle \theta^{\mu\nu} \rangle_0, \end{aligned} \quad (26)$$

where the subscript 0 refers to the trivial vacuum ($A = 1$ and $B = 0$). The bag constant is defined by the difference $\epsilon = \frac{1}{4} \langle \theta_\mu^\mu \rangle - \frac{1}{4} \langle \theta_\mu^\mu \rangle_0$ and after computing the integral becomes

$$\epsilon = -\frac{M_V^4 N_f N_c}{192\pi^2}. \quad (27)$$

The formula implies that it costs energy to dig a hole in the vacuum with a non-vanishing pion weak decay constant (see Eq. (24)), as one might expect for the chirally symmetric broken phase.

D. Two-point correlators in the meson sector

In SQM the quark propagator has no poles but cuts at $p^2 = M_V^2/4$ preventing the occurrence of quarks on

the mass shell. This complies to the notion of analytic confinement, a necessary but certainly not sufficient condition for color confinement. This non-standard behavior already suggests a possible departure from the standard treatment. However, to justify the claim of confinement one should check, in addition, the absence of cuts in physical correlators. Note that this question is in principle unrelated to the analytic confinement of bound quarks in a soliton with baryon number one which will be discussed in further sections below, but it is still interesting to see the analytic properties of the model. We analyze this issue below in some detail for the two-point mesonic correlators defined as

$$\Pi_{AB}(q) = i \int d^4x e^{-iq \cdot x} \langle 0 | T \{ J_A(x) J_B(0) \} | 0 \rangle, \quad (28)$$

where $J_A(x)$ and $J_B(x)$ are interpolating currents with the relevant meson quantum numbers. In the standard path integral approach (see Eq. (8)) the time-ordered products of currents in the vacuum can be evaluated by suitable functional derivatives of the generating functional (10) with respect to external bosonic currents, and in the large- N_c limit the path integral is driven to the saddle point of the path integral in the presence of those currents. On the other hand, at large N_c any two-point mesonic correlation function should have the general structure [2, 3]

$$\Pi_J(q^2) = \sum_n \frac{f_{J,n}^2}{M_{J,n}^2 - q^2} \quad (29)$$

due to confinement. This is a very stringent test, since it implies in particular a meromorphic analytic structure in the q^2 complex plane. Amazingly, this rather simple requirement has never been accomplished in chiral quark models, either local or nonlocal³.

A straightforward consequence of the large- N_c representation of the two point correlator in Eq. (29) is *positivity*, $\Pi_J(q^2) > 0$, in the Euclidean region $q^2 = -Q^2 < 0$ and *quark unitarity* at large values of q^2 . This ensures that, for instance, the inclusive $e^+e^- \rightarrow \text{hadrons}$ total cross section is proportional to the imaginary part of the polarization operator in the vector channel.⁴

In our previous work [53] we have evaluated the VV and AA correlators corresponding to the conserved vector and axial currents

$$J_V^{\mu,a}(x) = \bar{q}(x) \gamma^\mu \frac{\lambda_a}{2} q(x), \quad (30)$$

$$J_A^{\mu,a}(x) = \bar{q}(x) \gamma^\mu \gamma_5 \frac{\lambda_a}{2} q(x) \quad (31)$$

for a general spectral function $\rho(\omega)$ using solutions to the Ward-Takahashi identities based on the gauge technique. In this paper we use the effective action (10) to evaluate the correlation functions. Details of the calculation are provided in Appendix A. We find

$$\Pi_{VV}^{\mu a, \nu b}(q) = \frac{1}{2} \delta_{ab} (g^{\mu\nu} q^2 - q^\mu q^\nu) \Pi_V^T(q^2), \quad (32)$$

with⁵

$$\Pi_V^T(q^2) = \frac{2N_c}{3q^2} \int \rho(\omega) d\omega \times \left\{ 2\omega^2 (I(q^2, \omega) - I(0, \omega)) - q^2 \left(\frac{1}{48\pi^2} - I(q^2, \omega) \right) \right\}, \quad (33)$$

and

$$\Pi_{AA}^{\mu a, \nu b}(q) = \frac{1}{2} \delta_{ab} (g^{\mu\nu} q^2 - q^\mu q^\nu) \Pi_A^T(q^2), \quad (34)$$

with

$$\Pi_A^T(q^2) = \Pi_V^T(q^2) + 4N_c \int d\omega \omega^2 \rho(\omega) I(q^2, \omega). \quad (35)$$

In the particular case of the meson dominance model for the spectral function, Eq. (19), up to an (infinite) constant one has a remarkably simple result

$$\begin{aligned} \Pi_V^T(q^2) &= \frac{f_V^2}{M_V^2 - q^2} - \frac{N_c}{24\pi^2} \log \left(1 - \frac{q^2}{M_V^2} \right), \\ \Pi_A^T(q^2) &= -\frac{f^2}{q^2} - \frac{N_c}{24\pi^2} \log \left(1 - \frac{q^2}{M_V^2} \right), \end{aligned} \quad (36)$$

where $f_V^2 = f^2$. The above formulas clearly display the ρ meson pole in the vector channel and the pion pole in the axial channel. Also, we see that $f_A^2 = 0$, *i.e.*, there is no axial meson dominance. Our expressions fulfill the first Weinberg sum rule,

$$\lim_{q^2 \rightarrow 0} q^2 [\Pi_V^T(q^2) - \Pi_A^T(q^2)] = f^2. \quad (37)$$

Similarly as in other local quark models, the second Weinberg sum rule is not satisfied,

$$\lim_{q^2 \rightarrow -\infty} q^4 [\Pi_V^T(q^2) - \Pi_A^T(q^2)] = -M_V^2 f^2 \neq 0, \quad (38)$$

as noted in our previous work [53]. Since the second Weinberg sum rule is a high-energy feature of the theory, one hopes that it is not crucial for the low-energy phenomena studied in this paper and in particular for the soliton properties which probe Euclidean momenta corresponding to a soliton size $\sim \sqrt{6}/M_V$ (see, *e.g.*, Eq. (98) below). This assumption has implicitly

³ Instead, calculations at large values of Q^2 have only been confronted to QCD sum rules (see, *e.g.*, Ref. [47] and references therein.)

⁴ This asymptotic quark unitarity holds for external currents and should not be confused with the S-matrix hadron unitarity which is violated at any finite order of the large N_c expansion due to the $1/\sqrt{N_c}$ suppressed behavior of the meson-meson couplings.

⁵ We correct here a typo in our previous work [53], Eq. (4.3). Our conventions here are $\Pi_V^T(q^2) = -2\Pi(q^2)/q^2$.

been made in state-of-the-art chiral quark soliton models [24, 25, 26, 27, 28].

The presence of the log pieces in the correlators guarantees the fulfillment of quark unitarity since⁶

$$\text{Im}\Pi_V^T(q^2) = \text{Im}\Pi_A^T(q^2) = \frac{N_c}{24\pi}, \quad q^2 > M_V^2. \quad (39)$$

The appearance of these quark unitarity cuts can be inferred from the general structure of the quark propagator (see Eq. (21)) for any quark momentum $p^2 > M_V^2/4$, in spite of the fact that there are no poles in the quark propagator. A more detailed analysis is presented in Appendix B. Note that in QCD one obtains these parton-like relations for $q^2 \rightarrow \infty$. We stress that the coefficients of the log terms are precisely such as in the one-loop QCD calculation, complying to the parton-hadron duality. Moreover, despite the unconventional features of SQM involving complex masses, *positivity* is preserved both for the pole and for the cut contributions to the imaginary parts of the considered correlators, as can be seen from Eq. (36). This is a virtue of the spectral model, not easily fulfilled in other chiral quark models⁷. It is important to realize that this quark unitarity relation is hidden in the large- N_c meromorphic representation of Eq. (29) at large q^2 through the asymptotic density of $\bar{q}q$ states [70].

To see this we may compare to the large- N_c Regge models (see e.g. [71] and references therein), where the meson spectrum is chosen to be a tower of infinitely many radially excited states with masses $M_{n,V}^2 = M_V^2 + 2\pi\sigma n$, where σ is the string tension and the residue is taken to be constant $f_{n,V}^2 = N_c\sigma/(12\pi)$ precisely to implement quark-hadron duality at large q^2 . As we see, SQM corresponds to keeping one pole in the vector channel and approximating the higher states by a logarithm. More explicitly, one has

$$\begin{aligned} \Pi_V(q^2) - \Pi_V(0) &= \frac{N_c\sigma}{12\pi} \sum_{n=0} \left[\frac{1}{M_V^2 + 2\pi\sigma n - q^2} - \frac{1}{M_V^2 + 2\pi\sigma n} \right] \\ &= \frac{N_c}{24\pi^2} \left[\Psi\left(\frac{M_V^2 - q^2}{2\pi\sigma}\right) - \Psi\left(\frac{M_V^2}{2\pi\sigma}\right) \right], \end{aligned}$$

where the digamma function, $\Psi'(z) = \Gamma'(z)/\Gamma(z)$ has been introduced. SQM corresponds to representing the

⁶ We define the discontinuity as

$$\text{Disc}\Pi(q^2) = \Pi(q^2 + i0^+) - \Pi(q^2 - i0^+) = 2i\text{Im}\Pi(q^2).$$

⁷ For instance, the Pauli-Villars regularization spoils positivity due to subtractions, while dispersion relations are fulfilled. The proper-time regularization preserves positivity but does not fulfill dispersion relations due to a plethora of complex poles [69].

infinite Regge sum

$$\Psi(1+z) - \Psi(1) = - \sum_{n=1}^{\infty} \left[\frac{1}{n+z} - \frac{1}{n} \right], \quad (40)$$

where $-\Psi(1) = \gamma$ is the Euler-Mascheroni constant, by the approximation of taking explicitly the first pole. The higher poles lead to the asymptotic behavior

$$-1/(z+1) + 1 + \log(1+z), \quad (41)$$

approximated by the cut in SQM. The accuracy is better than 20 % for $0 < z < \infty$. We also recall that the large- N_c analyses restricted to a finite number of resonances [72, 73] provide a meromorphic structure but fail to give the large- q^2 parton-hadron duality conditions.

For completeness we also discuss the scalar and pseudoscalar channels, where the currents are given by

$$J_S^a(x) = \bar{q}(x) \frac{\lambda_a}{2} q(x), \quad (42)$$

$$J_P^a(x) = \bar{q}(x) i\gamma_5 \frac{\lambda_a}{2} q(x). \quad (43)$$

No Ward-Takahashi identities may be written for these currents and thus they are not directly amenable to the gauge technique. The effective action approach used here is superior to the gauge technique since it also allows to compute the two-point correlators not directly related to conserved currents. The result is given up to two subtraction terms as follows (see Appendix A). Defining

$$\begin{aligned} \Pi_{SS}^{ab}(q) &= \frac{1}{2} \delta^{ab} \Pi_S(q), \\ \Pi_{PP}^{ab}(q) &= \frac{1}{2} \delta^{ab} \Pi_P(q) \end{aligned} \quad (44)$$

one gets

$$\begin{aligned} \Pi_S(q^2) &= \frac{N_c}{8\pi^2} q^2 \log\left(1 - \frac{q^2}{M_V^2}\right), \\ \Pi_P(q^2) &= \frac{N_c}{8\pi^2} q^2 \log\left(1 - \frac{q^2}{M_V^2}\right) - \frac{2f^2 M_V^2}{M_V^2 - q^2} \\ &\quad + \frac{2\langle\bar{q}q\rangle}{f^2} \frac{1}{q^2} \frac{M_S^4(M_V^2 - q^2)}{M_V^2(M_S^2 - q^2)^2}, \end{aligned} \quad (45)$$

where the residue of the pion pole is $2f^2 B_0^2$, with $B_0 = -\langle\bar{q}q\rangle/f^2$. We see that $f_S = 0$, *i.e.*, there is no excited pseudoscalar meson dominance. Again, the emergence of the quark unitarity cuts is manifest. Similarly to the vector and axial correlators, the first $SS - PP$ Weinberg-like sum rule is verified

$$\lim_{q^2 \rightarrow 0} q^2 [\Pi_S(q^2) - \Pi_P(q^2)] = -2B_0^2 f^2, \quad (46)$$

while the second $SS - PP$ sum rule is not,

$$\lim_{q^2 \rightarrow -\infty} q^2 [\Pi_S(q^2) - \Pi_P(q^2)] = -2M_V^2 f^2 \neq 0. \quad (47)$$

Our analysis of both the second Weinberg sum rules for $VV - AA$ and $SS - PP$ correlators agrees with the observed mismatch of the low-energy coefficients L_8 and L_{10} between SQM [55] and the large- N_c evaluation in the single-resonance approximation (SRA) [72, 73] (where both sum rules are enforced). In [55] it was also shown that matching L_3 of both SQM and the large- N_c SRA yields the identity between the scalar and meson masses, $M_S = M_V$ (as we assume for the rest of the paper). It is interesting that the same condition also follows from the requirement of having a single pole in the PP correlator, Eq. (45). Moreover, at small q^2 one has

$$\Pi_V(q) - \Pi_A(q) = \frac{f^2}{q^2} - 4L_{10} + \dots, \quad (48)$$

$$\Pi_S(q) - \Pi_P(q) = -2B_0^2 \left[\frac{f^2}{q^2} + 16L_8 + \dots \right]. \quad (49)$$

Using Eqs. (36) and (45) and taking $M_S = M_V$ yields

$$\begin{aligned} L_8 &= \frac{N_c}{384\pi^2} - \frac{f^6}{16\langle\bar{q}q\rangle^2}, \\ L_{10} &= -\frac{N_c}{92\pi^2}, \end{aligned} \quad (50)$$

in agreement with results from the derivative expansion carried out in [55]. The large- N_c SRA yields $L_8 = 3f^2/(32M_S^2)$ and $L_{10} = -3f^2/(8M_V^2)$ [72, 73], while the large- N_c Regge models produce $L_{10} = -N_c/(96\sqrt{3}\pi)$.⁸

To summarize this section, SQM provides meson two-point correlators which carry poles as well as cuts, while strictly speaking large N_c requires only having poles. Thus, despite the quark propagator not having poles, the meson correlations do not exhibit true confinement. Although we cannot prove it in general for any correlation function, all two-point correlators we have considered obey positivity and analyticity, *i.e.* dispersion relations. This is required by the (asymptotic) quark unitarity and causality, *i.e.* the current commutators must vanish outside the causal cone, $[j(x), j(0)] = 0$ for $x^2 < 0$. The coefficients of the log terms are in agreement with the parton-hadron duality. On the other hand, the second Weinberg sum rule is not satisfied, as in other local chiral quark models. This calls for caution, in particular when analyzing processes sensitive to high-momenta.⁹

⁸ At the mean field level in a gradient expansion the L_8 term corresponds to $\mathcal{O}(m^4)$ corrections to the soliton energy, while L_{10} couples to external axial and vector currents. So a slight mismatch in these values should not influence strongly the mean field soliton properties. We estimate the corresponding correction to the energy as $\Delta E_8 = \Delta L_8 4m_\pi^4 \int d^3x [\cos(2\theta(r)) - 1] \sim -3\text{MeV}$, with $\Delta L_8 \sim 10^{-3}$ – a negligible number.

⁹ We remind that nonlocal models do indeed fulfill this high energy constraint [39] and the violation of the second Weinberg sum rule in local models is probably related to the violation of the two body consistency conditions discussed above (see Sects. II A and Sect. II B). On the other hand it is uncertain if nonlocal models do indeed satisfy analyticity.

E. The topological current

In a previous work [55] it was shown how the Wess-Zumino-Witten term arises for SQM in the *presence* of the spectral regularization. As a sample calculation illustrating the consistency condition of Sect. II A we compute the baryon current in the limit of spatially large backgrounds. This also shows how the regularization effects cancel in the final result, yielding the well known Goldstone-Wilczek current [4]. Taking the appropriate functional derivative in Eq. (2) we find

$$\begin{aligned} \langle \bar{q}(x) \gamma^\mu q(x) \rangle &= i \frac{1}{Z} \frac{\delta Z}{\delta v_\mu(x)} \Big|_0 \\ &= \lim_{x' \rightarrow x} (-i)^2 \frac{1}{Z} \frac{\delta}{\delta \eta(x)} \gamma^\mu \frac{\delta Z}{\delta \bar{\eta}(x')} \Big|_0 \\ &= \int_C d\omega \rho(\omega) \text{tr} \left[\gamma^\mu \langle x | \frac{-i}{i\cancel{\partial} - \omega U^5} | x \rangle \right]. \end{aligned} \quad (51)$$

The first two lines display the consistency condition. The derivative expansion of the Dirac operator can be neatly done with the help of the identity

$$\langle x | \frac{1}{i\cancel{\partial} - \omega U^5} | x \rangle = \text{tr} \int \frac{d^4 k}{(2\pi)^4} \frac{1}{\not{k} + i\cancel{\partial} - \omega U^5}, \quad (52)$$

where the differential operator acts to the right on the function $f(x) = 1$. This formula can be justified through the use of an asymmetric version of the Wigner transformation presented in Ref. [74]. Formal expansion in powers of ∂ yields

$$\begin{aligned} \langle x | \frac{1}{i\cancel{\partial} - \omega U^5} | x \rangle &= \sum_{n=0}^{\infty} \text{tr} \int \frac{d^4 k}{(2\pi)^4} \left[\frac{1}{k^2 - \omega^2} \right]^{n+1} \\ &\quad (\not{k} + \omega U^{5\dagger}) [(-i\cancel{\partial}) (\not{k} + \omega U^{5\dagger})]^n. \end{aligned} \quad (53)$$

The leading non-vanishing term is

$$\begin{aligned} \langle \bar{q}(x) \gamma^\mu q(x) \rangle &= \int_C d\omega \rho(\omega) \int \frac{d^4 k}{(2\pi)^4} \times \\ &\quad \times \frac{\omega^4}{[k^2 - \omega^2]^4} \text{tr} \left[\gamma^\mu U^{5\dagger} (i\cancel{\partial} U^5)^3 \right] = \rho_0 B^\mu, \end{aligned} \quad (54)$$

where $B_\mu(x)$ is the topological Goldstone-Wilczek current,

$$B_\mu = \frac{1}{24\pi^2} \epsilon^{\alpha\beta\mu\nu} \langle (U^\dagger \partial_\alpha U) (U^\dagger \partial_\beta U) (U^\dagger \partial_\nu U) \rangle, \quad (55)$$

and

$$\begin{aligned} \rho_0 &= (-96\pi^2 i) \int_C d\omega \rho(\omega) \int \frac{d^4 k}{(2\pi)^4} \frac{\omega^4}{[k^2 - \omega^2]^4} \\ &= \int_C d\omega \rho(\omega) = 1, \end{aligned} \quad (56)$$

where in the first line we have computed the momentum integral and in the second line used the normalization

condition (17). Thus the proper normalization of the spectral function is responsible for the correct topological properties in SQM, preservation of anomalies, *etc.* In fact, we view the uniform treatment of the anomalous processes as one of the main advantages of SQM over other local chiral quark models.

III. BUILDING THE BARYON

In this section we show how valence orbits are constructed in SQM. The issue is far from trivial, as unlike the case of local models, there is no obvious Fock space representation. Already the experience of nonlocal models showed that the construction of valenceness is an involved issue [48, 49]. There a bound-state pole of the propagator was found in the background of hedgehog chiral fields, and this state was occupied with $N_c = 3$ valence quarks. The full contribution to the baryon current (local and nonlocal) yielded a correct (and quantized) baryon number of the soliton. In the present case we face a different situation, with the spectral density and inherent complex masses present. Thus we start our derivation from very basic field-theoretic foundations, arriving in the end at a very simple prescription holding under plausible assumptions concerning the analyticity properties of the valence eigenvalue as a function of the complex mass.

A. Interpolating baryon fields

In the standard field-theoretic approach a baryon can be described in terms of the corresponding correlation function

$$\Pi_B(x, x') = \langle 0 | T \{ B(x) \bar{B}(x') \} | 0 \rangle \quad (57)$$

with $B(x)$ denoting an interpolating baryonic operator in terms of anti-commuting quark fields. We take the simplest combination

$$B(x) = \frac{1}{N_c!} \epsilon^{\alpha_1, \dots, \alpha_{N_c}} \Phi^{a_1, \dots, a_{N_c}} q_{\alpha_1 a_1}(x) \cdots q_{\alpha_{N_c} a_{N_c}}(x), \quad (58)$$

where $(\alpha_1, \dots, \alpha_{N_c})$ are the color indices, (a_1, \dots, a_{N_c}) the spinor-flavor indices, and $\Phi^{a_1, \dots, a_{N_c}}$ is the appropriate completely symmetric spinor-flavor amplitude. Inserting a complete set of baryon eigenstates gives

$$\begin{aligned} \Pi_B(x, x') = & \quad (59) \\ & \theta(t - t') \sum_n \langle 0 | B(0) | B_n, \vec{k} \rangle \langle B_n, \vec{k} | \bar{B}(0) | 0 \rangle e^{-i(x-x')k} \\ & + (-1)^{N_c} \theta(t' - t) \sum_n \langle 0 | \bar{B}(0) | \bar{B}_n, \vec{k} \rangle \langle \bar{B}_n, \vec{k} | B(0) | 0 \rangle \\ & \times e^{+i(x-x')k}, \end{aligned}$$

where B_n (\bar{B}_n) are the baryon (antibaryon) states with momentum \vec{k} . Next we take the limit $t - t' = T \rightarrow -i\infty$. That way the lightest baryon at rest is selected in the sum,

$$\Pi_B(x, x') = \langle 0 | B(0) | B \rangle \langle B | \bar{B}(0) | 0 \rangle e^{-iT M_B}. \quad (60)$$

In the large- N_c limit, we first rewrite the time ordered product as a path integral over the fermionic degrees of freedom with the weight $\exp(iS_{\text{SQM}})$. The resulting expression, in turn, can be obtained by the appropriate functional differentiation of the generating functional $Z[s, p, v, a, \eta, \bar{\eta}]$ with respect to the external quark fields $\eta(x)$ and $\bar{\eta}(x)$, yielding

$$\begin{aligned} \Pi_B(x, x') = & \Phi^{a_1, \dots, a_{N_c}} \bar{\Phi}^{a'_1, \dots, a'_{N_c}} \\ & \times \int DU e^{i\Gamma[U]} \prod_{i=1}^{N_c} i S_{a_i a'_i}(x, x'). \end{aligned} \quad (61)$$

Here the one-particle Green function in SQM is given by

$$S_{aa'}(x, x') = \int_{C'} d\omega \rho(\omega) \langle x | (i\partial - \omega U^5)^{-1}_{aa'} | x' \rangle \quad (62)$$

and the one loop effective action has the form

$$\Gamma[U] = -i N_c \int_{C'} d\omega \rho(\omega) \text{Tr} \log (i\partial - \omega U^5). \quad (63)$$

Note the presence of the spectral integration, however, the contour C' to be used in the baryon sector is yet to be determined. There is no a priori reason why it should be equal to the vacuum contour C^{10} . The limit $N_c \rightarrow \infty$ drives the functional integral over the bosonic U fields into a saddle point. In the vacuum sector one then obtains the mean-field vacuum. In the baryon sector, due to the presence of N_c factors $S_{a,a'}$ in the numerator, the dominating saddle point configuration is of course different from that of the vacuum and depends non-trivially on x and x' . The limit of a large evolution time T selects the minimum-energy stationary configuration. For stationary configurations the Dirac operator can be written as

$$i\partial - \omega U^5 = \gamma_0(i\partial_t - H(\omega)), \quad (64)$$

with the Dirac Hamiltonian equal to

$$H(\omega) = -i\alpha \cdot \nabla + \omega U^5. \quad (65)$$

Note that the spectral mass ω appearing here is *complex* and the situation is unconventional, since $H(\omega)$ is

¹⁰ Note by analogy that in the standard many-body quantum field theory the contour in the complex *energy* variable selects the orbits to be occupied and is clearly different for states with different baryon number, or baryon density, where it crosses the real axis at the value of the chemical potential.

not *Hermitean*. In such a case one must distinguish between the right and left eigenvectors, $H\psi_n^R = \epsilon_n\psi_n^R$ and $H^\dagger\psi_n^L = \epsilon_n\psi_n^L$, not related by the Hermitean conjugation, i.e. $(\psi_n^R)^\dagger \neq \psi_n^L$. The orthogonality relation is $\langle\psi_n^L, \psi_m^R\rangle = \delta_{nm}$ and completeness is given in terms of the left-right identity $\sum |\psi_n^R\rangle\langle\psi_n^L| = 1$. We will not use this fancy notation, but will implicitly understand that ψ is the right eigenvector, while ψ^\dagger is in fact the complex-conjugated left eigenvector. The corresponding eigenvalue problem is then

$$H(\omega)\psi_n(\vec{x};\omega) = \epsilon_n(\omega)\psi_n(\vec{x};\omega). \quad (66)$$

For our particular Hamiltonian one has the following useful properties

$$\begin{aligned} H(\omega)^\dagger &= H(\omega^*), \\ \gamma_5 H(\omega) \gamma_5^{-1} &= H(-\omega), \\ \gamma_0 H(\omega) \gamma_0^{-1} &= -H(-\omega^*)^\dagger, \\ (\gamma_0 \gamma_5) H(\omega) (\gamma_0 \gamma_5)^{-1} &= -H(\omega), \\ \text{tr} H(\omega) &= 0. \end{aligned} \quad (67)$$

where the trace is in the Dirac sense. Some properties of the eigenvalues deduced from the properties (67) are

$$\begin{aligned} \epsilon_n(\omega)^* &= \epsilon_n(\omega^*), \\ \epsilon_n(\omega) &= \epsilon_n(-\omega). \end{aligned} \quad (68)$$

One can now use the spectral representation of the propagator

$$\begin{aligned} iS_{aa'}(\vec{x}, t; \vec{x}', t') &= \int_{C'} d\omega \rho(\omega) \\ &\times \int_\gamma \frac{d\nu}{2\pi} \sum_n \frac{e^{i\nu(t-t')}}{\nu - \epsilon_n(\omega)} \psi_{na}(\vec{x}; \omega) \bar{\psi}_{na'}(\vec{x}'; \omega) \end{aligned} \quad (69)$$

with $\psi_{na}(\vec{x}; \omega)$ ($\bar{\psi}_{na}(\vec{x}; \omega)$) and $\epsilon_n(\omega)$ denoting the right (left conjugated) eigenfunctions and eigenvalues of $H(\omega)$ evaluated at the stationary bosonic configuration. The contour for the energy integration, discussed in the following, is denoted by γ . For the calculation of the baryon state note that the propagator given by Eq. (69) and the fermion determinant given by Eq. (63) have to be evaluated at large Euclidean times.

B. Hedgehog ansatz

The stationary solutions of chiral quark models have the familiar hedgehog form,

$$U^5(\vec{x}) = \exp(i\gamma_5 \vec{\tau} \cdot \vec{\theta}(\vec{x})), \quad (70)$$

with $\vec{\theta}$ denoting the chiral phase field. In the hedgehog ansatz

$$\vec{\theta} = \hat{r}\theta(r), \quad (71)$$

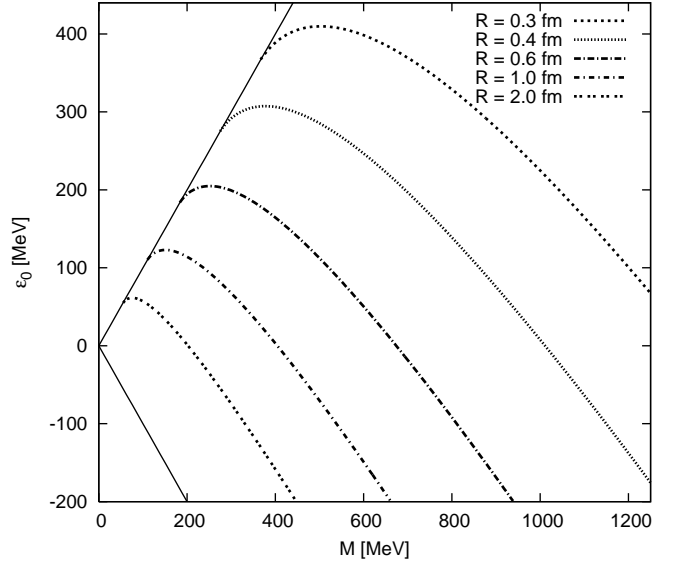


FIG. 2: The lowest $J^P = 0^+$ eigenvalue ϵ_0 as a function of mass M for several soliton size parameters R in the profile (72). The curves are arranged with the lowest value of R at the top. The two straight solid lines indicate the boundaries of the gap, M and $-M$. Each curve leaves the positive continuum at some critical value of M , assumes a maximum, and then decreases, asymptotically becoming parallel to the $-M$ line.

with $\theta(r)$ being a radial function. In the following two subsections we analyze the Dirac problem (66) for the exponential profile as an example,

$$\theta(r) = \pi e^{-r/R}, \quad (72)$$

In particular our figures are obtained for that case. Other popular cases include the linear profile

$$\theta(r) = \pi(1 - r/R)\theta(R - r) \quad (73)$$

and the arctan profile [20]

$$\theta(r) = 2\arctan(R/r)^2. \quad (74)$$

The parameter R is a generic size scale of the soliton proportional to the baryon rms radius. The profile (72) is in fact a fairly good approximation to the fully self-consistent profile found numerically in Sect. IV.

In the treatment of hedgehog systems it is relevant to consider symmetries such as the grand spin $G = I + J$, the sum of isospin and spin. The reader is referred to Refs. [24, 25, 26, 27] for necessary details.

C. The valence contribution

Now we resort to the numerical calculation of the spectrum in the chiral soliton, described in detail in the preceding sections. What we need for the present discussion

is the behavior of the spectrum when we vary the spectral mass ω as an independent variable. We focus on the grand-spin 0 parity + state, $G^P = 0^+$, where $G = I + J$ is the sum of isospin and spin, appropriate to classify states in the hedgehog background (71). In Fig. 2 we show the dependence of the lowest 0^+ eigenvalue on the mass parameter M for *real masses* (in our notation M is the same as real ω). Subsequent curves are obtained for the profile (72) with a fixed radius R . In fact, all the displayed curves are related to each other via simple scaling. Indeed, introducing $\tilde{\xi} = \vec{r}/R$ and $\Omega = \omega R$ we can rewrite the Dirac equation in the form

$$(-i\alpha \cdot \nabla_{\tilde{\xi}} + \Omega U^5(\tilde{\xi})) \Psi_n(\tilde{\xi}; \Omega) = E_n(\Omega) \Psi_n(\tilde{\xi}; \Omega), \quad (75)$$

which depends on a single scale Ω . By identification

$$\epsilon_n(\omega) = \frac{E_n(\omega R)}{R}. \quad (76)$$

As can be promptly seen from Fig. 2, for any value of R we have for the valence 0^+ level the limiting behavior

$$\epsilon_0(M) \sim M \quad \text{at} \quad M \rightarrow 0, \quad (77)$$

$$\epsilon_0(M) \sim -M + a \quad \text{at} \quad M \rightarrow \infty, \quad (78)$$

where a is a constant. Correspondingly, at fixed M in the limit of low R (small solitons) we have $\epsilon_0(M) \simeq M$, *i.e.* the level goes to the top of the gap, whereas in the limit of high R (large solitons) the behavior $\epsilon_0(M) \simeq -M + a$ shows that the level goes to the bottom of the gap. The small M behavior, together with the reflexion property Eq. (68) suggests a branch point behavior at the origin

$$\epsilon_0(\omega) \rightarrow \sqrt{\omega^2} \quad \omega \rightarrow 0 \quad (79)$$

which is no mystery, since it corresponds to a free particle with the complex mass and with energy $\sqrt{k^2 + \omega^2}$ at zero momentum. Unfortunately, in our study we only have access to the chiral soliton spectrum for real M , thus we do not possess the information on analyticity properties of the eigenvalues as functions of ω , which is fully accessible only in exactly soluble problems.

Indeed, due to the inherent numerical complications, finite-size discrete basis used, *etc.*, such information would be difficult to obtain numerically in a reliable way. Thus, we proceed motivated by the real mass results and the analogy to a similar exactly-solvable model presented in Appendix D. In other words, our assumptions made in the general hedgehog case appear to be justified.

Let us now review the calculation of the Dirac propagator for the standard case of a *real* mass. If we first compute the ν integral in Eq. (69), we have to consider the γ contour in the complex- ν space which for real masses and hence real eigenvalues has the standard form of going below the real axis for states with energy below the gap and going above the real axis for states above the gap. This yields

$$\int_{\gamma} \frac{d\nu}{2\pi i} \frac{e^{i\nu(t-t')}}{\nu - \epsilon_n(M)} = \quad (80)$$

$$[\theta(t-t')\theta(\epsilon_n(M)) - \theta(t'-t)\theta(-\epsilon_n(M))] e^{-i\epsilon_n(M)(t-t')},$$

hence the positive (negative) energy states propagate forward (backward) in time. This is equivalent to a damped (exploding) imaginary-time behavior for $t - t' \rightarrow \pm i\infty$. This real mass result coincides with the standard one. If we change M the valence level may change sign (because it is equivalent to changing the soliton size R and the level dives into the sea according to (78)). Thus, according to Eq. (80) one keeps the contour. If we deformed the contour deciding that we occupy the negative eigenvalue then the imaginary-time behavior implying the standard particle (antiparticle) interpretation would be violated.

Let us now analyze the case of a *complex* mass. For that purpose we go slightly off the real axis, $\omega = M + i\Gamma$, and expand

$$\epsilon_n(M + i\Gamma) = \epsilon_n(M) + i\Gamma\epsilon'_n(M) - \frac{1}{2}\Gamma^2\epsilon''_n(M) + \dots \quad (81)$$

The edges of the bound state gap and consequently the Dirac eigenvalues wander into the complex- ν plane moving upwards or downwards, depending on the sign of $\epsilon'_n(M)$. The eigenvalues fulfilling $\epsilon'_n(M) = 0$ stay stationary on the real axis. According to Fig. (2), we have $\epsilon''_0(M) < 0$ for any $M > 0$. The question is whether or not we should also deform the contour γ in the evaluation of the propagator (69). On the one hand, the eigenvalues lying in the complex plane should not cross the contour, as this would lead to discontinuities, thus some deformation must be done. On the other hand, if $\epsilon'_0(M) = 0$ we move along the real axis in the positive direction by the amount $-\frac{1}{2}\Gamma^2\epsilon''_0(M)$, Eq. (81), hence crossing the contour only in the case where also $\epsilon_0(M) = 0$. According to Fig. (2) this situation never happens unless $M = 0$ or M is much larger than the position of the maximum (which, as we will see, is of no relevance to our construction). Hence, we deform the contour in such a way that it continues to pass through the $\nu = 0$ point, but never allows a complex eigenvalue to intersect. Such a contour yields

$$\int_{\gamma} \frac{d\nu}{2\pi i} \frac{e^{i\nu(t-t')}}{\nu - \epsilon_n(\omega)} = [\theta(t-t')\theta(\text{Re } \epsilon_n(\omega)) - \theta(t'-t)\theta(-\text{Re } \epsilon_n(\omega))] e^{-i\epsilon_n(\omega)(t-t')}. \quad (82)$$

We note that the large imaginary time evolution is damped, as we might have expected. In the positive $t - t' > 0$ branch, where a baryon (and not an antibaryon) propagates, we are thus left with the integral

$$\int_{C'} d\omega \rho(\omega) \theta(\text{Re } \epsilon_n(\omega)) e^{-\tau \epsilon_n(\omega)}. \quad (83)$$

for the imaginary time $\tau \rightarrow \infty$. Note that we only have the positive section of the contour, as implied by the condition $\text{Re } \epsilon_n(\omega) > 0$. Recall that we wish to occupy the lowest 0^+ orbit with the eigenvalue $\epsilon_0(\omega)$. We proceed by using the *saddle-point* method. First we have to locate stationary points of $\epsilon_0(\omega)$, *i.e.* the points ω_m where

$$\epsilon'_0(\omega_m) = 0. \quad (84)$$

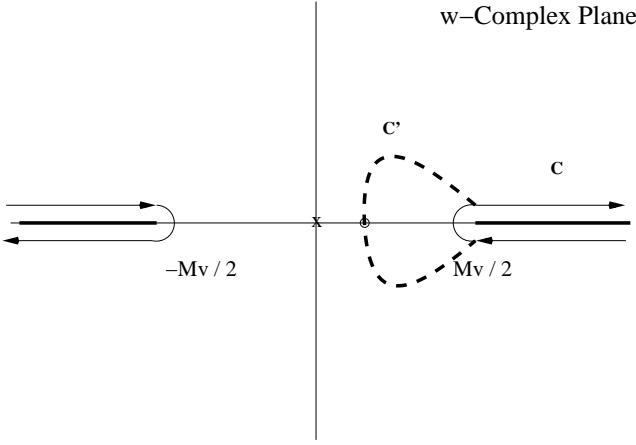


FIG. 3: The deformed contour C' in the complex ω -plane for the saddle-point evaluation of the valence contribution.

From Fig. 2 we find, that for any value of R there exists a saddle located at the maximum of the curve $\epsilon_0(M)$. We denote the position of the saddle as M_0 ¹¹. We call M_0 the *saddle mass*. As we move left from the saddle, decreasing M , we enter at some critical value M_c into the upper continuum. On the basis of the toy model results of Appendix D, we expect that $\epsilon_0(\omega)$ has a branch cut at $\omega = M_c$ running downwards. We observe from Fig. 2 that the saddles are located right of M_c for any value of the soliton size R .

In order to compute the integral in Eq. (83) we deform the original contour C used in the vacuum sector into the contour C' shown in Fig. 3. It contains the segment $C' - C$ (dashed line), which runs across $\omega = M_0$ parallel to the imaginary axis. Note that it is not necessary to change the path globally but only in the vicinity of the stationary point. Making the change of variables $\omega = M_0 + i\Gamma$, where M_0 is the saddle mass, $\epsilon'(M_0) = 0$ we get

$$\begin{aligned} & \int_{C'-C} d\omega \rho(\omega) \theta(\text{Re } \epsilon_n(\omega)) e^{-\tau \epsilon_n(\omega)} \\ & \rightarrow \int_{-\infty}^{\infty} i d\Gamma \rho(M_0) e^{-\tau \epsilon(M_0)} e^{\frac{1}{2} \tau \epsilon_n''(M_0) \Gamma^2} \\ & \sim i \rho(M_0) \sqrt{\frac{2\pi}{-\epsilon_n''(M_0) \tau}} e^{-\tau \epsilon(M_0)} \end{aligned}$$

¹¹ A priori we should admit multiple saddles ω_m . We choose the branch, denoted ω_0 , with the lowest possible real part of the eigenvalue. In addition, the complex reflexion property implies that if ω_0 is a saddle, then ω_0^* is also a saddle. As a consequence, for complex saddles the large Euclidean time behavior would not be purely exponential, but also some oscillations would set in. This obviously contradicts the spectral decomposition (60), which allows only for real stationary points. Therefore, although complex solutions may a priori exist, they should be considered a spurious result of the model. Similar problems occur also in the local models [69].

$$= Z_0 e^{-\tau \epsilon(M_0)} \quad (85)$$

where the wave function renormalization factor Z_0 has been included. Finally, we compare Eq. (85) to Eq. (60) and read off the valence contribution to the energy as

$$E_{\text{val}} = N_c \epsilon_0(M_0). \quad (86)$$

The necessary conditions are $\epsilon'_0(M_0) = 0$, $\epsilon_0(M_0) > 0$, and $\epsilon''_0(M_0) < 0$, all satisfied in our case, as shown in Fig. 2. In addition, the solution is only admissible with the conditions $M_c < M_0 < M_V/2$, which guarantee a real residue. As we have already discussed, $M_c < M_0$ holds for all values of R . For $M_0 > M_V/2$ we would have a complex residue, contradicting the spectral decomposition of the propagator, Eq. (60). According to Fig. 2, for the ansatz (72) this occurs for $R < 0.6$ fm, where no bound-state nucleon can be constructed. Thus, in the large imaginary time limit $t \rightarrow -i\infty$ and $t' \rightarrow +i\infty$ we get (see e.g. Eq. (85))

$$S(x', x) \rightarrow Z_0 \Psi_0(x) \bar{\Psi}_0(x') e^{-i(t-t')\epsilon_0}, \quad (87)$$

where Ψ_0 is the valence Dirac spinor.

To summarize, our prescription for the valence orbit consists of the following very simple steps:

1. Obtain (numerically) the spectrum for the valence orbital as a function of the real positive mass M .
2. Look for the saddle mass, *i.e.*, a maximum with respect to M , with the help of conditions $\epsilon'_0(M_0) = 0$ and $\epsilon''_0(M_0) < 0$. From analyticity, this is the saddle point which corresponds to the saddle mass M_0 .
3. If $M_c \leq M_0 < M_V/2$, the valence contribution to the soliton mass is $N_c \epsilon_0(M_0)$, otherwise there is no baryon state in the model.

There is an essential difference between the standard valence prescription based on the Fock-space decomposition, used in local quark models, and our prescription for SQM presented above. In the first case the size of the profile, R , and the quark mass, M , can be fixed independently in the Dirac operator, whereas in the present case we actually find a correlation between them. In the quark propagator we have a superposition of masses ω which are integrated over¹², thus no additional independent scale is present in the problem. An immediate consequence can be seen in Fig. 4, where we compare the valence eigenvalue for the profile function (60) along the manifold where $\epsilon'_0(M) = 0$ (for a given R) to the fixed-mass result of the local chiral quark model, obtained with

¹² This reminds of the familiar distinction between the phase and group velocities of wave packets made out of a continuous superposition of plane waves.

$M_Q = 300$ MeV. From the scaled Dirac equation (76) and our valence prescription it follows that

$$\epsilon_0 = k/R, \quad (88)$$

where k is a constant depending on the particular profile. In particular, for $R \rightarrow 0$ in SQM one has $\epsilon_0 \rightarrow 1/R$ (a signature of a “repulsive force”), as opposed to the behavior $\epsilon_0 \rightarrow M_Q$ of a free particle at rest in the case of the fixed-mass model. This means in practice that the bound state never becomes unbound in the presence of a chiral field background (see the discussion of Sect. III F) and reflects the absence of on-shell quarks in the vacuum (analytic confinement) in SQM. Another feature of SQM with our valence prescription is that the valence eigenvalue never dives into the negative part of the spectrum. The prescription for fixed-mass models allows the valence contribution to become negative, and this happens with a finite slope which originates from non-analyticity. This entering of the valence level into the negative part of the spectrum was interpreted within the chiral quark soliton model as entering the “Skyrme” model regime. In our approach such a regime never arises. However, the $1/R$ dependence of the valence contribution behaves very much like the Skyrme stabilizing term.

Similarly, the saddle mass scales as

$$M_0 = k'/R. \quad (89)$$

Numerically, for the exponential profile (72) one gets $k = 123$ MeV fm and $k' = 151$ MeV fm, for the linear profile (73) $k = 234$ MeV fm and $k' = 257$ MeV fm, and for the arctan profile (74) $k = 100$ MeV fm and $k' = 119$ MeV fm.

D. The soliton baryon density and the baryon number

A crucial point is to show that our soliton corresponds to a system with baryon number equal to one. This requires the separation between the valence and sea contributions to the baryon number. To analyze this point we have to compute the following time ordered product,

$$\begin{aligned} \Pi_B^\mu(x, x', y) &= \langle 0 | T \left\{ B(x) \bar{q}(y) \gamma^\mu q(y) \bar{B}(x') \right\} | 0 \rangle \\ &= \frac{\delta}{\delta v_\mu(y)} \Pi_B^v(x, x') \Big|_0 \end{aligned} \quad (90)$$

with $B(x)$ denoting the interpolating baryonic operator, Eq. (58) and $\Pi_B^v(x, x')$ the baryon correlator (57) in the presence of a external vector field $v^\mu(y)$ for which the result (61) follows if the external source is included in the propagator

$$S_{aa'}^v(x, x') = \int_C d\omega \rho(\omega) \langle x | (i\bar{\partial} - \not{\partial} - \omega U^5)^{-1}_{aa'} | x' \rangle. \quad (91)$$

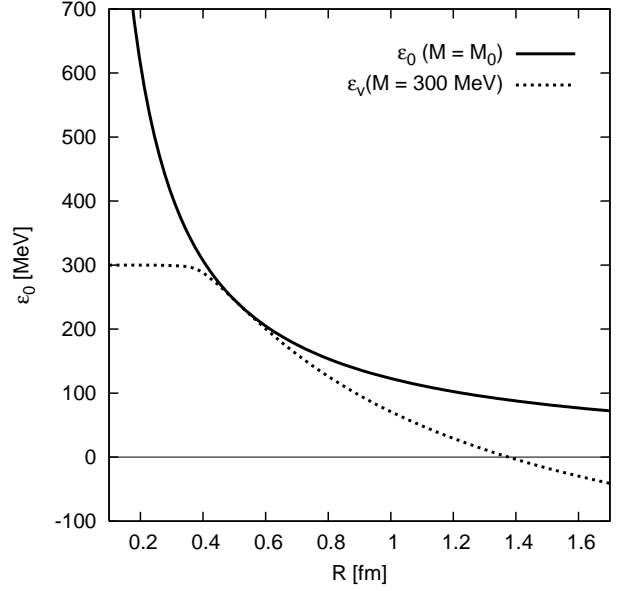


FIG. 4: Solid line: the valence eigenvalue ϵ_0 and the saddle mass, M_0 , for the 0^+ state (maxima of Fig. 2), plotted as a function of the soliton size R . Dotted line: the 0^+ eigenvalue ϵ at the fixed value of $M = 300$ MeV, as used in traditional fixed-mass models. We note that the SQM prescription has $\epsilon_0 = \text{const}/R$, whereas $\epsilon \rightarrow \text{const}$ at $R \rightarrow 0$ and becomes negative at $R \rightarrow \infty$.

For the open line propagator the functional derivative can be readily evaluated yielding

$$\begin{aligned} \frac{\delta S^v(x', x)}{\delta v_\mu(y)} \Big|_0 &= \int_C d\omega \rho(\omega) \\ &\times \langle x | \frac{1}{i\bar{\partial} - \omega U^5} | y \rangle \gamma^\mu \langle y | \frac{1}{i\bar{\partial} - \omega U^5} | x' \rangle \\ &\rightarrow \bar{\Psi}_0(y) \gamma^\mu \Psi_0(y) S(x, x') \end{aligned} \quad (92)$$

where in the last line the limit $t \rightarrow -i\infty$ and $t' \rightarrow +i\infty$ has been taken along the line of reasoning developed in Sec. III C (see Eq. 87). The determinant contribution to the baryon current can be deduced from Eq. (51). Collecting all results we obtain for the three-point correlator in the asymptotic limit the factorized form

$$\Pi_B^\mu(x, x', y) \rightarrow B^\mu(y) \Pi_B(x, x') \quad (93)$$

with the total baryon current given by

$$\begin{aligned} B^\mu(x) &= \bar{\Psi}_0(x) \gamma^\mu \Psi_0(x) \\ &+ \int_C d\omega \rho(\omega) \text{tr} \left[\gamma^\mu \langle x | \frac{-i}{i\bar{\partial} - \omega U^5} | x \rangle \right] \end{aligned} \quad (94)$$

which is our result for the baryon current and in general for any observable based on a one-body operator. In Fig. 5 the sea and the valence contributions to the baryon density for several soliton radii in the SQM are displayed. As we see, the Dirac sea contribution gives a vanishing contribution to the baryon number; only the valence

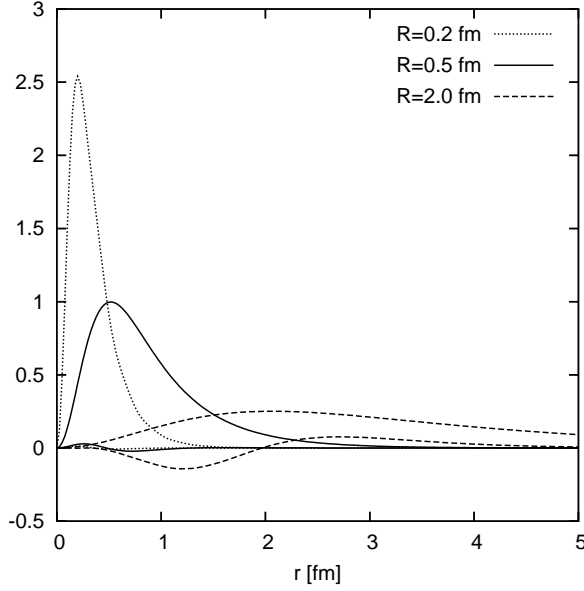


FIG. 5: Sea and valence contribution to the radial baryon density for several soliton radii in the SQM (the valence parts have positive sign at all r).

quarks contribute to the total normalization. This is consistent with our finding that the valence level never dives into the negative energy region.

It is worth mentioning that the previous calculation can be extended mutatis mutandis to any one body observable and in particular to the energy-momentum tensor. In the following section we analyze the sea contribution as it arises from Eq. (60) onwards. A non trivial check which results from the one body consistency condition is that such a calculation coincides with the one based on the energy-momentum tensor in the soliton background.

E. The sea contribution

To identify the sea contribution we compare, as done for the valence case, the spectral decomposition of the two point correlator at large Euclidean times, Eq. (60), with the path integral representation, Eq. (61). Using Eq. (63) for stationary configurations, the Dirac sea contribution to the energy is obtained by the spectral integration along the original contour C of Fig. 1,

$$\begin{aligned}
 E_{\text{sea}} &= \frac{i}{T} N_c \int_C d\omega \rho(\omega) \text{Tr} \log (i\cancel{\partial} - \omega U^5) \\
 &= -N_c \int_C d\omega \rho(\omega) \frac{1}{2} \sum_n \sqrt{\epsilon_n(\omega)^2} \\
 &= N_c \int_C d\omega \rho(\omega) \sum_{i \in \text{sea}} \epsilon_i(\omega), \quad (95)
 \end{aligned}$$

where T is the time and n indicates all (positive- and negative-energy) states of the Dirac Hamiltonian H de-

fined in Eq. (65) and the frequency integral has been carried out. In the last line Eq. (67) has been used and summation i runs over negative energy (sea) states only. A full-fledged evaluation of this quantity is presented in Sect. IV. To understand the general trend we will present an estimate based on the so-called *two point function approximation* (TPA) proposed originally in Ref. [20] and further exploited in Ref. [75, 76]. This approximation has the virtue of reproducing both the limit of large and small soliton sizes and is based in the identity for the normal parity contribution to the action

$$\begin{aligned}
 &\int_C d\omega \rho(\omega) \text{Tr} \log (i\cancel{\partial} - \omega U^5) |_{n.p.} \\
 &= \frac{1}{2} \int_C d\omega \rho(\omega) \text{Tr} \log (\partial^2 + i\omega \cancel{\partial} U^5 + \omega^2) \quad (96)
 \end{aligned}$$

(deduced by commuting the γ_5 matrix across the Dirac operator) and further expanding the logarithm to second order in the field U^5 , yielding

$$\begin{aligned}
 E_{\text{sea}}^{\text{TPA}} &= \frac{-iN_c}{4T} \int_C d\omega \rho(\omega) \text{Tr} \left\{ \left[\frac{1}{\partial^2 + \omega^2} i\omega \cancel{\partial} U^5 \right]^2 \right\} \\
 &= \frac{-iN_c}{T} \int_C d\omega \rho(\omega) \int \frac{d^4 q}{(2\pi)^4} q^2 I(q^2, \omega) \omega^2 \langle |U(q)|^2 \rangle \quad (97)
 \end{aligned}$$

where the functional trace and Dirac traces have been evaluated, $\langle . \rangle$ indicates the isospin trace, and $U(q)$ is the Fourier transform of the chiral field $U(x)$ (see Appendix A for notation). The one-loop integral $I(q^2, \omega)$ is introduced and calculated in Appendix B. A straightforward calculation in the meson-dominance version of the SQM for static fields yields

$$E_{\text{sea}}^{\text{TPA}} = \frac{1}{4} f_\pi^2 \int \frac{d^3 q}{(2\pi)^3} \bar{q}^2 \langle |U(\vec{q})|^2 \rangle \frac{M_V^2}{\bar{q}^2 + M_V^2}, \quad (98)$$

where

$$U(\vec{q}) = \int d^3 x U(\vec{x}) e^{i\vec{q} \cdot \vec{x}}. \quad (99)$$

The factor appearing in Eq. (98) is the pion form factor, Eq. (18) in the space-like region, $q^2 = -\mathbf{q}^2 < 0$. Actually, this is a general feature, static soliton profiles probe the Euclidean region of mesonic correlation functions. At large values of the soliton size R , small values of q dominate in Eq. (98) and one gets

$$E \sim a f_\pi^2 R, \quad (100)$$

where a is a numerical constant. For the exponential profile (72) one gets numerically $a = 30.99$. In the opposite limit of small soliton sizes, large q values dominate and Eq. (98) yields

$$E \sim b f_\pi^2 R (M_V R)^2, \quad (101)$$

with $b = 28.11$. This behavior is different from the $R^3 \log R$ short distance behavior documented in Ref. [20] for the proper-time regularized fermion determinant; it is also free of the $R \log R$ behavior reported in Ref. [77, 78] for the renormalized sea energy, which generated a vacuum Landau instability.

F. Existence of absolute minima

The total soliton energy is the valence plus the sea contribution as

$$E_B = E_{\text{val}} + E_{\text{sea}}. \quad (102)$$

At small radii the valence contribution (88) dominates and $E \sim 1/R$, while at large radii the Dirac sea contribution dominates and $E \sim R$. Since the function $E(R)$ is continuous, on these simple grounds we prove to have a minimum. The behavior is illustrated in Fig. (6), where we show the energy dependence as a function of the profile size R for the profile (72). For this restricted configuration one clearly sees the occurrence of an *absolute minimum* as a consequence of the fact that the valence quarks never become unbound. In contrast, in the standard approach to chiral quark solitons the valence quarks become unbound at small R and one has instead a *local minimum*, which becomes unstable when the total soliton energy exceeds that of N_c free quarks at rest, $E > N_c M$. This instability has been an obvious cause of concern since this situation corresponds to bound but not confined solitons. In practice, it would not be a problem if valence states were deeply bound. However, most calculations have produced solutions which lie on the unstable branch. The fact that our solutions correspond to an absolutely stable state is a remarkable property of SQM together with our construction of the valence state. Results for other profiles of the chiral field are qualitatively similar to the case of Fig. 6.

Another interesting feature that can be seen from a direct comparison of Figs. 6 and 4 is that the minimum takes place at a soliton size R where the valence state for our model and the fixed-mass models produce a similar dependence. This suggests that the constituent fixed mass in soliton models may indeed correspond to a given saddle mass in the spectral construction and that the shallow (and unstable) minima found there may indeed be identified as the absolute and stable minima obtained here.

IV. RESULTS FOR THE SELF-CONSISTENT SOLITON

In this section we describe the numerical properties of self-consistent chiral solitons in SQM, as well as the corresponding observables.

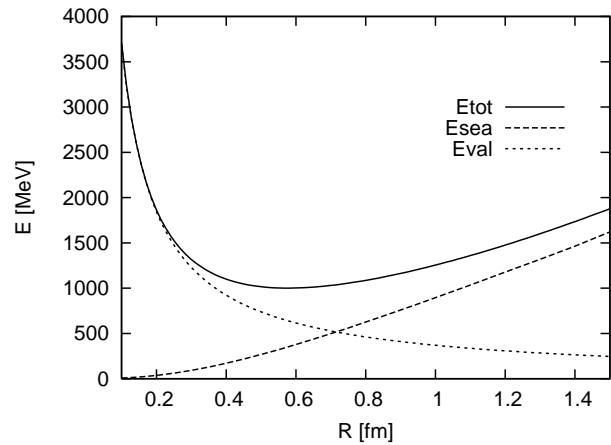


FIG. 6: Total energy of the soliton (solid line) and its valence and sea components for the profile (72), plotted as functions of R . An absolute minimum exists.

A. Evaluation of observables

As is well known, observables in hedgehog solitons fall into two categories: independent of and dependent on *cranking* [79]. The second case is much more complicated, hence in this paper we deal only with the quantities that do not involve cranking. Observables independent of cranking can be written in terms of single spectral sums of the form

$$A = \sum_i A_i, \quad (103)$$

where A is the value of the observable in the soliton, and A_i is the single-particle contribution which includes a valence orbit and the Dirac sea. In the spectral approach this is generalized, in the sense that an extra integration over the spectral variable ω is present. With our method of treating the valenceness we also have a separated contribution from N_c occupied valence states,

$$\begin{aligned} A &= A_{\text{val}} + A_{\text{sea}}, \\ A_{\text{val}} &= N_c A(\omega_{\text{val}}), \\ A_{\text{sea}} &= \int_C d\omega \rho(\omega) A_{\text{sea}}(\omega), \end{aligned} \quad (104)$$

where val and sea indicate valence and sea, $\omega_{\text{val}} = M_0$ is the saddle mass, $\rho(\omega)$ is the spectral function consisting of the vector and scalar parts given in Eq. (20), and $A_{\text{sea}}(\omega) = \sum_{i \in \text{sea}} A_i(\omega)$ with $A_i(\omega)$ denoting the ω -dependent single-particle value of the observable in the orbit i . Due to the hedgehog symmetries for the observables in question one may replace the sum over the negative energy states, $\sum_{i \in \text{sea}}$, with $1/2$ of the sum over all states, $\frac{1}{2} \sum_{n \in \text{all}}$.

The contour C is invariant under the transformation

$\omega \rightarrow -\omega$, see Fig. 1. Therefore

$$\begin{aligned} A_{\text{sea}} &= \frac{1}{2} \left[\int_C d\omega \rho(\omega) A_{\text{sea}}(\omega) - \int_C d\omega \rho(-\omega) A_{\text{sea}}(-\omega) \right], \\ &= \int_C d\omega \rho_V(\omega) \frac{A_{\text{sea}}(\omega) + A_{\text{sea}}(-\omega)}{2} \\ &\quad + \int_C d\omega \rho_S(\omega) \frac{A_{\text{sea}}(\omega) - A_{\text{sea}}(-\omega)}{2}, \end{aligned} \quad (105)$$

where ρ_V and ρ_S are the odd and even parts of the spectral function ρ , respectively, see Eq. (20). As we have stressed before, the contour C in Fig. 1 is complex. This is a complication, since in a numerical calculation we obviously do not have access to $A(\omega)$ in the complex ω plane. For that reason we use a method which allows us to carry on the calculation along the real axis in the ω plane, as explained in Appendix F. According to the formalism of Sect. III, the energy of the soliton is

$$\begin{aligned} E &= N_c E_{\text{val}} + \frac{d^2}{du^2} [E_V(u) + E_S(u)] \Big|_{u=1/M_V^2}, \\ \bar{E}_{V,S}(u) &= 2 \int_{1/(2\sqrt{u})}^{\infty} d\omega \text{disc}[\bar{\rho}_{V,S}(\omega)] \\ &\quad \times \sum_i \frac{\epsilon_i(\omega, m) \pm \epsilon_i(-\omega, m)}{2}. \end{aligned} \quad (106)$$

With the help of Eq. (F15) we may also write

$$\begin{aligned} \bar{E}_{V,S}(u) &= 2 \int_{1/(2\sqrt{u})}^{\infty} d\omega \text{disc}[\bar{\rho}_{V,S}(\omega)] \\ &\quad \times \sum_i \frac{\epsilon_i(\omega, m) \pm \epsilon_i(\omega, -m)}{2}. \end{aligned} \quad (107)$$

In the chiral limit

$$\begin{aligned} \bar{E}_V(u) &= 2 \int_{1/(2\sqrt{u})}^{\infty} d\omega \text{disc}[\bar{\rho}_V(\omega)] \sum_i \epsilon_i(\omega, 0), \\ \bar{E}_S(u) &= 0. \end{aligned} \quad (108)$$

All observables not involving cranking can be evaluated with the technique described above and with the help of “standard” formulas at each ω . The derivatives with respect to u are carried out numerically.

B. Self-consistent equations

Now we present some details of our self-consistent procedure. We use the linear representation of the hedgehog field, $U = s + i\hat{r} \cdot \vec{\tau} p$, and impose the nonlinear constraint $s^2 + p^2 = 1$ by renormalizing the fields after each numerical iteration. The Euler-Lagrange equations for the radial s and p fields are obtained from Eq. (G1) and have the form

$$\frac{s(r)}{g^2} = N_c \bar{\psi}_0(\vec{x}, M_0) \psi_0(\vec{x}, M_0)$$

$$\begin{aligned} &+ \int_C d\omega \rho(\omega) \sum_i \bar{\psi}_i(\vec{x}, \omega) \psi_i(\vec{x}, \omega), \\ \frac{p(r)}{g^2} &= N_c \bar{\psi}_0(\vec{x}, M_0) i\gamma_5 \vec{\tau} \cdot \hat{r} \psi_0(\vec{x}, M_0) \\ &+ \int_C d\omega \rho(\omega) \sum_i \bar{\psi}_i(\vec{x}, \omega) i\gamma_5 \vec{\tau} \cdot \hat{r} \psi_i(\vec{x}, \omega), \end{aligned} \quad (109)$$

where g^2 is treated as a Lagrange multiplier. The first terms on the r.h.s. are the valence contributions, evaluated according to the SQM prescription. The second terms are the Dirac sea contributions, where the sum over the negative-energy states i is carried out, or, equivalently, it can be replaced by 1/2 of the sum over all states. With the help of formulas (F10, F11) the spectral integration in (109) can be performed as a real-valued integral. The spinors $\psi_i(\vec{x}, \omega)$ are obtained by solving the Dirac equation in the background of the fields $s(r)$ and $p(r)$ at a given value of ω .

The code used to find numerically the self consistent solutions is a modification of the method used in solving different versions of chiral-quark models. The quark orbits are calculated by diagonalizing H for each value of ω in the discrete Kahana-Ripka basis [16]. The Euler-Lagrange equations are solved by iteration. The numerical effort involved in the calculation is similar to that in the case of solitons in non-local models [48, 49].

C. The self-consistent solution

For the sake of obtaining physical properties of the soliton, we use two versions of the model. The first one (model I) is just the standard meson-dominance SQM, with the single vector meson mass, $M_V = m_\rho = 769$ MeV. This model (in the chiral limit) has only one scale, thus all observables are proportional to the value of M_V in appropriate power. In particular, $f_\pi^2 = M_V^2/(8\pi^2)$. The second model (model II) includes also the excited ρ state, $\rho'(1465)$. The spectral function is taken to be the weighted sum of Eq. (20), containing 90% of the ground-state ρ , and 10% of excited ρ . All quantities are distributive over the spectral density, *e.g.* $f_\pi^2 = 0.9m_\rho^2/(8\pi^2) + 0.1m_{\rho'}^2/(8\pi^2)$. Model II contains two scales, and produces somewhat heavier and more compact solitons, as expected on simple scaling grounds. We work with the physical pion, $m_\pi = 139.6$ MeV, and the current quark mass is adjusted such that the GMOR relation is fulfilled, $m\langle\bar{q}q\rangle = m_\pi^2 f_\pi^2$.

The results of the self-consistent calculation for the case with physical pion mass are displayed in Table I and in Fig. 7. The chiral corrections are small and do not alter our basic conclusions. We note that for both models the value of the saddle mass M_0 is well below the critical value $\frac{1}{2}M_V$ discussed in Sect. III.

Comparing the soliton energy to the experimental nucleon mass we should be aware that our soliton is a mean-field solution with grand spin 0 and should not

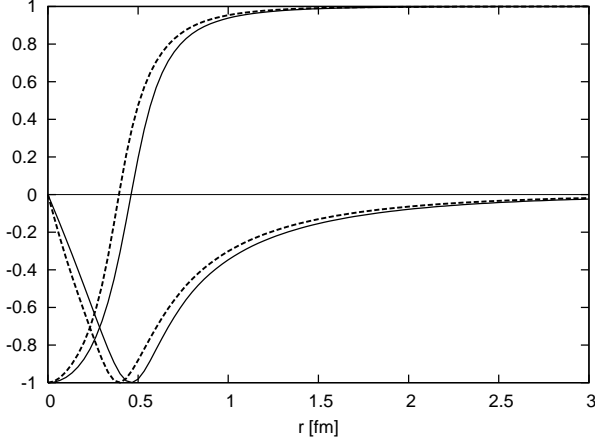


FIG. 7: The $s \equiv \cos \theta$ and $p \equiv \sin \theta$ fields as a function of the radius r for the two self-consistent solutions of Table I: the solid lines for the model I and the dashed lines for model II.

be identified with the nucleon, but rather with the average of the mass of the nucleon and the $\Delta(1232)$ isobar $\frac{1}{2}(M_N + M_\Delta) = 1174$ MeV. Moreover, quantization of the collective coordinates, or projection of the soliton wave function on the subspace with good quantum numbers [80, 81], reduces its energy by eliminating the spurious rotational and translational energy. We note that the contribution to the energy arising from the scalar spectral density, $E_{\text{sea},S}$, is much smaller than the vector part, $E_{\text{sea},V}$. Furthermore, we notice that the model gives approximate equipartition of energy between each valence quark and the Dirac sea, in agreement to the $1/R$ behavior of the valence contribution and the approximate $\sim R$ dependence of the sea part.

	model I	model II
f_π [MeV]	86.5	97.3
m_π [MeV]	139.6	139.6
$(-\langle \bar{q}q \rangle)^{1/3}$ [MeV]	243	243
m [MeV]	5.04	6.37
M_0 [MeV]	267	304
ε_0 [MeV]	233	263
$E_{\text{sea},V}$ [MeV]	285	351
$E_{\text{sea},S}$ [MeV]	36	35
E_{total} [MeV]	1019	1174

TABLE I: Model parameters and the soliton energy in the self-consistent calculation with the physical pion mass.

D. Results for observables

As discussed in Sec. IV, in the present approach we deal only with those observables that do not involve

	model I	model II	experiment
$\sqrt{\langle r^2 \rangle_{I=0,\text{val}}}$ [fm]	1.23	1.07	-
$\sqrt{\langle r^2 \rangle_{I=0,\text{total}}}$ [fm]	1.24	1.08	0.79
$g_A(\text{val})$	0.79	0.79	-
$g_A(\text{total})$	0.93	0.95	1.26
$\mu_{I=1}(\text{val})$	2.40	2.07	-
$\mu_{I=1}(\text{total})$	2.96	2.67	4.71
$\sigma_{\pi N}$ [MeV]	36	33	45 ± 8

TABLE II: Properties of the self-consistent solution of Table I: the rms isoscalar charge radius, the axial-vector charge g_A , the isovector magnetic moment $\mu_{I=1}$, and the sigma commutator $\sigma_{\pi N}$. The valence contribution (val) is given separately. The contribution from the sea (not given explicitly) is dominated by the vector part, similarly as in the case of the energy. The experimental value of $\sigma_{\pi N}$ is taken from Ref. [82].

cranking. Inclusion of cranking, which requires a linear-response calculation, is numerically involved and is outside of the scope of this study. In Table II we display some characteristic observables of the self consistent solution for the choice of parameters of Table I. Firstly, we note that the isoscalar rms charge radius of the soliton is too large as compared to the experiment. This quantity is dominated by the valence contribution, as can also be seen from Fig. 8. The quark spinors of the valence wave function exhibit a long tail which is a feature related to our prescription for constructing the valence orbit. The large r behavior is of the form $\exp(-\sqrt{M_0^2 - \epsilon_0^2} r)$, and in our case the value of $\kappa = \sqrt{M_0^2 - \epsilon_0^2}$ is small, with $\kappa = 1/(1.5 \text{ fm})$ in model I and $\kappa = 1/(1.3 \text{ fm})$ in model II. The large soliton radius can perhaps be reduced by subtracting the spurious center-of-mass motion of the soliton. Including higher vector mesons in the model tends to reduce the soliton size, as expected by scaling arguments, however, on the expense of increasing f_π and E_{total} .

In the evaluation¹³ of g_A and the isovector magnetic moment $\mu_{I=1}$ we use the semiclassical projection coefficients as obtained in the large- N_c limit [79]. Both values are lower than the corresponding experimental values. But since our solution is dominated by the valence state we could as well, instead of the semiclassical projection, use the quark model wave functions for evaluation of the valence parts of observables. Then the expectation value of the $\sigma\tau$ operator for the proton and the neutron yields the coefficient $\frac{5}{9}$ instead of $\frac{1}{3}$. That would result in higher values, in better agreement with the experiment. The value of the sigma commutator, which in our model is equal to

$$\sigma_{\pi N} = -m_\pi^2 f_\pi^2 \int d^3r (s(r) - 1) \quad (110)$$

¹³ Explicit expressions for these quantities may be found, *e.g.*, in Ref. [26, 27].

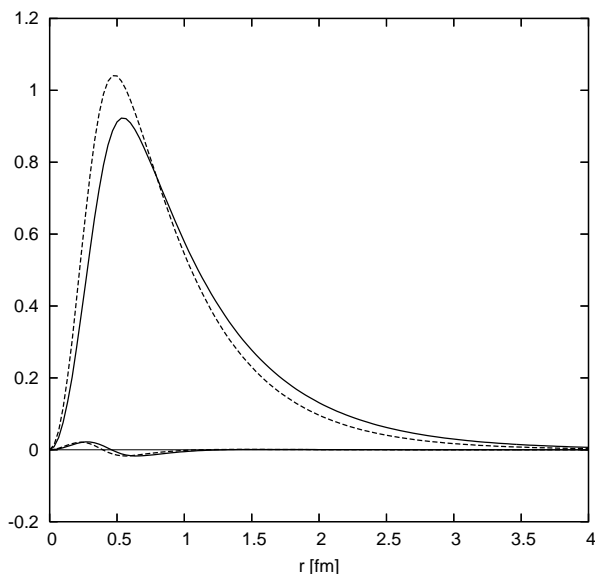


FIG. 8: The valence and the sea contributions to the baryon density (multiplied by $4\pi r^2$) for the self-consistent solutions: the solid lines for model I and the dashed lines for model II.

is reasonably well reproduced, assuming values somewhat smaller than the experimental number, showing that the spatial extent of our chiral profile is not too large.

The results for the observables turn out to be quite similar to those obtained in other chiral models. In particular, they are strikingly close to the predictions of the model with the non-local regulators [48, 49].

V. CONCLUSION

For many years it has been accepted that baryons arise as solitons of a chiral Lagrangean in the large- N_c -limit of QCD. However, the precise realization of this attractive and fruitful idea is still unclear. Many model Lagrangeans have been proposed, emphasizing different aspects of the problem and incorporating as many known features of the underlying quark-gluon dynamics as possible. While on the one hand the Skyrme soliton models incorporate confinement but not the spin-1/2 partons, on the other hand, chiral quark soliton models account for spin-1/2 partons but lack the confinement property. This unsatisfactory situation has been calling for improvement. As a first and hopefully useful step, we have considered a model where quark poles on the real axis are absent, be it in the vacuum or in the soliton. Unfortunately, confinement does not hold since basic large- N_c requirements on the analytic structure of meson correlators are violated, similarly to other effective quark models. On the other hand the Spectral Quark Model provides a framework with spin-1/2 partons in the vacuum which simultaneously allows for baryonic soliton solutions cor-

responding to absolute minima of the action and hence cannot decay into three free quarks, unlike previous local chiral quark soliton models. This is due to the rather peculiar features of the model characterized by a continuous superposition of masses in the complex plane with a suitable spectral function. As a necessary complementary study we have examined an instance of an involved complex-mass relativistic system.

The solitons we find fit nicely into the phenomenological expectations of more standard chiral quark solitons with full inclusion of the polarized Dirac sea. In contrast to constituent chiral quark models where one is allowed to tune the constituent quark mass as a free parameter, the Spectral Quark Model does not have this freedom. In our case the vector meson mass determines one unique solution in the chiral limit and thus all properties scale with this mass. Actually, due to the superposition of complex spectral masses ω , in the soliton calculation there appears a saddle mass, M_0 , defined as a stationary point of the valence quark eigenvalue as a function of ω in a fixed soliton profile. In the chiral limit M_0 also scales with the vector meson mass and thus is a fixed number. To some extent the saddle mass behaves as a constituent quark mass determined uniquely by the soliton, and its numerical value comes out within the expected range $M_0 \sim 300\text{MeV}$ for the typical solitons minimizing the total energy. Moreover, the close resemblance of the valence contribution to the energy around the minimum suggests that the phenomenology and results of previous calculations within constituent chiral quark models with a constant mass are reproduced, at least for the low-lying baryon states. The new aspect unveiled by our calculation is the possibility of studying the monopole vibrations and their quantization which are the traditional candidate for describing excited baryonic states such as, *e.g.*, the Roper resonance. While studies of this sort are routinely carried out in the Skyrme model, the lack of confinement in the traditional chiral quark soliton model has prevented, as a matter of principle, calculations of excited states.

One distinguishing feature of the Spectral Quark Model construction is the verification of an important consistency relation involving quark two-point functions which were not fulfilled for fixed constituent mass chiral quark models. This feature, in addition to the uniform treatment of regularization removes theoretical doubts on the proper computation of the high-energy processes as regards their partonic interpretation and normalization. As we have mentioned, one motivation for using chiral quark soliton models is the spin 1/2 nature of the constituents, which makes the calculation of partonic distributions in the nucleon possible as a matter of principle. The results found in the present paper pave the way for such a calculation in the soliton picture where the interplay between the analyticity enforced by the lack of on-shell quarks and the chiral symmetry may simultaneously be tested for the low-lying baryon states.

Acknowledgments

This research is supported by the Polish Ministry of Education and Science, grants 2P03B 02828, by the Spanish Ministerio de Asuntos Exteriores and the Polish Ministry of Education and Science, project 4990/R04/05, by the Spanish DGI and FEDER funds with grant no. FIS2005-00810, Junta de Andalucía grants no. FQM225-05, EU Integrated Infrastructure Initiative Hadron Physics Project contract no. RII3-CT-2004-506078 and by the Bilateral Program for Scientific and Technological Cooperation of the Ministries of Science, Technology, and Higher Education of Poland and Slovenia.

APPENDIX A: THE EFFECTIVE ACTION TO SECOND ORDER IN THE FIELDS

When using the path integral (8) with the effective action (10) it is enough to expand the action to second order in the external sources and the dynamical pion field,

$$U = 1 + \frac{i}{f} \vec{\tau} \cdot \vec{\pi} \gamma_5 - \frac{1}{2f^2} \vec{\pi} \cdot \vec{\pi} + \dots \quad (\text{A1})$$

This can be done by noting that the Dirac operator in Eq. (11) can be decomposed as a free part plus a perturbation,

$$i\mathbf{D} = i\cancel{\partial} - \omega - V, \quad (\text{A2})$$

where

$$V = \omega \left(\frac{i}{f} \vec{\tau} \cdot \vec{\pi} \gamma_5 - \frac{1}{2f^2} \vec{\pi} \cdot \vec{\pi} + \dots \right) + \hat{m}_0 - (\not{p} + \not{p} \gamma_5 - s - i\gamma^5 p). \quad (\text{A3})$$

Note that *both* the free propagator and the potential V may depend on the spectral mass ω . Then the perturbative expansion of the fermion determinant can be readily done, yielding

$$\begin{aligned} i\Gamma &= N_c \int_C d\omega \rho(\omega) \text{Tr} \log(i\cancel{\partial} - \omega) \\ &- N_c \int_C d\omega \rho(\omega) \sum_{n=1}^{\infty} \frac{1}{n} \text{Tr} \left[\frac{1}{i\cancel{\partial} - \omega} V \right]^n \\ &= i\Gamma^{(0)} + i\Gamma^{(1)} + i\Gamma^{(2)} + \dots, \end{aligned} \quad (\text{A4})$$

which can be classified according to the number of external sources as well as dynamical fields.

The zeroth order contribution yields the vacuum energy,

$$\begin{aligned} i\Gamma^{(0)} &= N_c \int_C d\omega \rho(\omega) \text{Tr} \log(i\cancel{\partial} - \omega) \\ &= N_c N_f \int d^4x \int_C d\omega \rho(\omega) \int \frac{d^4p}{(2\pi)^4} \text{tr} \log(\not{p} - \omega) \\ &= \int d^4x \left\{ -\epsilon + N_c N_f \int \frac{d^4p}{(2\pi)^4} \text{tr} \log(\not{p}) \right\}, \end{aligned} \quad (\text{A5})$$

where the vacuum energy density, ϵ , defined relative to the case of massless quarks, has been explicitly separated. This quantity was computed in Ref. [53] and in Sec. II C of the present paper through the use of the energy momentum tensor. It is instructive to check the calculation in the effective action formalism. We use the reflection symmetry $p \rightarrow -p$ and the standard identity for matrices, $\text{tr} \log A + \text{tr} \log B = \log \det A + \log \det B = \log \det(AB) = \text{tr} \log(AB)$ for the commuting Dirac matrices $A = \not{p} - \omega$ and $B = \not{p} + \omega$ (in four dimensions $\det A = \det(-A)$). The vacuum energy density can be written as one half of any of these contributions. The Dirac trace becomes trivial and after interchanging the order in the momentum and spectral integrals one gets

$$\begin{aligned} \epsilon &= -2iN_c N_f \int \frac{d^4p}{(2\pi)^4} \\ &\times \int_C d\omega \rho(\omega) [\log(p^2 - \omega^2) - \log(p^2)]. \end{aligned} \quad (\text{A6})$$

To evaluate first the ω -integral we write

$$\log(p^2 - \omega^2) = \int^{p^2} \frac{dk^2}{k^2 - \omega^2}. \quad (\text{A7})$$

Thus, we readily get from direct application of Eq. (21),

$$\begin{aligned} \epsilon &= -2iN_c N_f \int \frac{d^4p}{(2\pi)^4} \int^{p^2} dk^2 \left[A(k^2) - \frac{1}{k^2} \right] \\ &= iN_c N_f \int \frac{d^4p}{(2\pi)^4} [p^2 A(p^2) - 1], \end{aligned} \quad (\text{A8})$$

after going to the Euclidean space and integrating by parts. The surface term has been discarded, as the condition $\lim_{s \rightarrow \infty} s^3 A(-s) = 0$, holds in the meson dominance realization Eq. (21). Thus the final result is finite,

$$\begin{aligned} \epsilon &= -\frac{N_c N_f M_V^4}{192\pi^2} = -(0.2\text{GeV})^4 \quad (N_f = 3) \\ &= -\frac{3N_f \pi^2 f^4}{N_c}, \end{aligned} \quad (\text{A9})$$

in agreement with Eq. (27) based on the energy-momentum tensor.

Returning to Eq. (A4), the first non-vanishing correction involves only the scalar source, yielding

$$\begin{aligned} i\Gamma^{(1)} &= N_c \int_C d\omega \rho(\omega) \text{Tr} \left\{ \frac{1}{i\cancel{\partial} - \omega} s \right\} \\ &= 4N_c \int \frac{d^4p}{(2\pi)^4} \int_C d\omega \frac{\rho(\omega)}{p^2 - \omega^2} \int d^4x \langle s(x) \rangle \end{aligned} \quad (\text{A10})$$

($\langle \cdot \rangle$ means the flavor trace), whence the quark condensate may be obtained as

$$N_f \langle \bar{q}q \rangle = -4iN_c N_f \int \frac{d^4p}{(2\pi)^4} B(p^2), \quad (\text{A11})$$

which becomes an identity according to Eq. (21).

Finally, the second order contribution can be written as

$$\begin{aligned}\Gamma^{(2)} &= \Gamma_{SS} + \Gamma_{PP} + \Gamma_{VV} + \Gamma_{AA} + \Gamma_{\pi\pi} \\ &+ \Gamma_{\pi P} + \Gamma_{\pi A} + \Gamma_{PA}.\end{aligned}\quad (\text{A12})$$

The calculation is straightforward. For the bilinears in the fields, generically written as $\varphi(x) = \varphi_A(x)\Gamma^A$ with A denoting Lorentz-flavor index, we have

$$\begin{aligned}i\Gamma^{(2)} &= -\frac{1}{2}N_c \int d\omega \rho(\omega) \text{Tr} \left[\varphi_A \Gamma^A \frac{1}{i\not{\partial} - \omega} \varphi_B \Gamma^B \frac{1}{i\not{\partial} - \omega} \right] \\ &= \frac{i}{2} \int \frac{d^4 q}{(2\pi)^4} \bar{\varphi}_A(q) \bar{\varphi}_B(-q) K_{AB}(q^2),\end{aligned}\quad (\text{A13})$$

where

$$(-i)K_{AB}(q) = -N_c \int_C d\omega \rho(\omega) \int \frac{d^4 p}{(2\pi)^4}$$

$$\times \text{Tr} \left[\Gamma_A \frac{i}{\not{p} - \not{q} - \omega} \Gamma_B \frac{i}{\not{p} - \omega} \right]. \quad (\text{A14})$$

The Fourier-transformed fields are defined through the relation

$$\varphi(x) = \int \frac{d^4 q}{(2\pi)^4} e^{iq \cdot x} \bar{\varphi}(q). \quad (\text{A15})$$

The flavor trace is trivial, $\langle \lambda_a \lambda_b \rangle = \delta_{ab}/2$. After using the vanishing condition of the positive moments, Eq. (23), the calculation of the Dirac trace and momentum integration yields

$$\begin{aligned}(-i)K_{SS}^{ab}(q) &= -N_c \int_C d\omega \rho(\omega) \int \frac{d^4 p}{(2\pi)^4} \text{Tr} \left[\frac{\lambda^a}{2} \frac{i}{\not{p} - \not{q} - \omega} \frac{\lambda^b}{2} \frac{i}{\not{p} - \omega} \right] \\ &= \delta^{ab} N_c \int_C d\omega \rho(\omega) [2I(0, \omega) \omega^2 + I(q^2, \omega)(4\omega^2 - q^2)],\end{aligned}\quad (\text{A16})$$

$$\begin{aligned}(-i)K_{PP}^{ab}(q) &= -N_c \int d\omega \rho(\omega) \int \frac{d^4 p}{(2\pi)^4} \text{Tr} \left[\frac{i}{\not{p} - \not{q} - \omega} i\gamma_5 \frac{\lambda^a}{2} \frac{i}{\not{p} - \omega} i\gamma_5 \frac{\lambda^b}{2} \right] \\ &= \delta^{ab} N_c \int_C d\omega \rho(\omega) [2I(0, \omega) \omega^2 - I(q^2, \omega) q^2],\end{aligned}\quad (\text{A17})$$

$$\begin{aligned}(-i)K_{VV}^{a\mu; b\nu}(q) &= -N_c \int d\omega \rho(\omega) \int \frac{d^4 p}{(2\pi)^4} \text{Tr} \left[\frac{i}{\not{p} - \not{q} - \omega} \gamma_\mu \frac{\lambda^a}{2} \frac{i}{\not{p} - \omega} \gamma_\nu \frac{\lambda^b}{2} \right] \\ &= \frac{1}{3} \delta^{ab} N_c \left(-g^{\mu\nu} + \frac{q^\mu q^\nu}{q^2} \right) \int_C d\omega \rho(\omega) \left[4I(0, \omega) \omega^2 - \frac{q^2}{24\pi^2} - 2I(q^2, \omega)(2\omega^2 + q^2) \right],\end{aligned}\quad (\text{A18})$$

$$\begin{aligned}(-i)K_{AA}^{a\mu; b\nu}(q) &= -N_c \int d\omega \rho(\omega) \int \frac{d^4 p}{(2\pi)^4} \text{Tr} \left[\frac{i}{\not{p} - \not{q} - \omega} \gamma_\mu \gamma_5 \frac{\lambda^a}{2} \frac{i}{\not{p} - \omega} \gamma_\nu \gamma_5 \frac{\lambda^b}{2} \right] \\ &= \frac{1}{3} \delta^{ab} N_c \left(-g^{\mu\nu} + \frac{q^\mu q^\nu}{q^2} \right) \int_C d\omega \rho(\omega) \left[4I(0, \omega) \omega^2 - \frac{q^2}{24\pi^2} + 2I(q^2, \omega)(4\omega^2 - q^2) \right] \\ &\quad - \delta^{ab} 4N_c \frac{q^\mu q^\nu}{q^2} \int_C d\omega \rho(\omega) I(q^2, \omega) \omega^2,\end{aligned}\quad (\text{A19})$$

$$\begin{aligned}(-i)K_{AP}^{a\mu; b}(q) &= -N_c \int d\omega \rho(\omega) \int \frac{d^4 p}{(2\pi)^4} \text{Tr} \left[\frac{i}{\not{p} - \not{q} - \omega} \gamma_\mu \gamma_5 \frac{\lambda^a}{2} \frac{i}{\not{p} - \omega} i\gamma_5 \frac{\lambda^b}{2} \right] \\ &= \delta^{ab} 2iN_c q^\mu \int_C d\omega \rho(\omega) \omega I(q^2, \omega),\end{aligned}\quad (\text{A20})$$

$$\begin{aligned}(-i)K_{\pi\pi}^{ab}(q) &= -N_c \int d\omega \rho(\omega) \int \frac{d^4 p}{(2\pi)^4} \text{Tr} \left[\frac{i\omega}{f^2} \delta^{ab} \frac{i}{\not{p} - \omega} + \frac{i}{\not{p} - \not{q} - \omega} \frac{\omega}{f} \gamma_5 \lambda^a \frac{i}{\not{p} - \omega} \frac{\omega}{f} \gamma_5 \lambda^b \right] \\ &= -\delta^{ab} 4N_c \frac{q^2}{f^2} \int_C d\omega \rho(\omega) \omega^2 I(q^2, \omega),\end{aligned}\quad (\text{A21})$$

$$\begin{aligned}(-i)K_{A\pi}^{a\mu; b}(q) &= -N_c \int d\omega \rho(\omega) \int \frac{d^4 p}{(2\pi)^4} \text{Tr} \left[\frac{i}{\not{p} - \not{q} - \omega} \gamma_\mu \gamma_5 \frac{\lambda^a}{2} \frac{i}{\not{p} - \omega} i\gamma_5 \lambda^b \frac{\omega}{f} \right] \\ &= -\delta^{ab} 4iN_c \frac{q^\mu}{f} \int_C d\omega \rho(\omega) I(q^2, \omega) \omega^2,\end{aligned}\quad (\text{A22})$$

$$\begin{aligned}
(-i)K_{P\pi}^{ab}(q) &= -N_c \int d\omega \rho(\omega) \int \frac{d^4 p}{(2\pi)^4} \text{Tr} \left[\frac{i}{\not{p} - \not{q} - \omega} i\gamma_5 \frac{\lambda^a}{2} \frac{i}{\not{p} - \omega} i\gamma_5 \lambda^b \frac{\omega}{f} \right] \\
&= \delta^{ab} 2N_c \frac{1}{f} \int_C d\omega \rho(\omega) [2I(0, \omega)\omega^3 - I(q^2, \omega)q^2\omega].
\end{aligned} \tag{A23}$$

where the basic one-loop two-point integral $I(q^2, \omega)$ is defined in Eq. (B1).

To compute the correlation functions as functional derivatives we must take into account the contributions from the pion pole. This is accomplished in a standard way by eliminating the pion field at the mean field level through the equations of motion, $\delta\Gamma/\delta\pi^a(x) = 0$, yielding at lowest order in the field

$$\pi^a(q)K_{\pi\pi}^{ab}(q) + p^a(q)K_{\pi P}^{ab}(q) + a^{a,\mu}(q)K_{A\pi}^{a,\mu;b}(q) = 0 \tag{A24}$$

and reinserting the pion field into the effective action $\Gamma^{(2)}$. This contribution exactly cancels the non-transverse piece of the AA correlator, reproducing the gauge technique result of Eq. (36) and an additional pion pole contribution to the PP correlator yielding Eq. (45).

APPENDIX B: USEFUL INTEGRALS

The basic two-point integral is given by¹⁴

$$\begin{aligned}
I(q^2, \omega) &= \frac{1}{i} \int \frac{d^4 k}{(2\pi)^4} \frac{1}{k^2 - \omega^2} \frac{1}{(q - k)^2 - \omega^2} \\
&= \frac{1}{i} \int \frac{d^4 k}{(2\pi)^4} \int_0^1 \frac{dx}{[k^2 - \omega^2 + q^2 x(1 - x)]^2} \\
&= -\frac{1}{(4\pi)^2} \int_0^1 dx \log [\omega^2 - x(1 - x)q^2].
\end{aligned} \tag{B1}$$

For the meson dominance case one can use the moments method, based on expansion in powers of q^2 and resummation of the series. This method provides a useful check to our computations. However, for the purpose of illustrating the issues of quark unitarity with our unconventional propagator it is enlightening to provide general formulas in terms of the vector and scalar components of the quark propagator. The ω integrals can be evaluated first by using Eqs. (21). We get the useful identities,

$$\begin{aligned}
A'(p^2) &= -\int_C d\omega \frac{\rho(\omega)}{[p^2 - \omega^2]^2}, \\
B'(p^2) &= -\int_C d\omega \frac{\omega \rho(\omega)}{[p^2 - \omega^2]^2}, \\
A(p^2) + p^2 A'(p^2) &= -\int_C d\omega \frac{\omega^2 \rho(\omega)}{[p^2 - \omega^2]^2},
\end{aligned}$$

$$B(p^2) + p^2 B'(p^2) = -\int_C d\omega \frac{\omega^3 \rho(\omega)}{[p^2 - \omega^2]^2}. \tag{B2}$$

The normalization of the pion field yields

$$f^2 = 4N_c i \int \frac{d^4 k}{(2\pi)^4} \frac{d}{dk^2} [k^2 A(k^2)] = \frac{M_V^2 N_c}{24\pi^2}. \tag{B3}$$

We also have

$$\begin{aligned}
&\int_C d\omega \rho(\omega) I(q^2, \omega) = \\
&i \int_0^1 dx \int \frac{d^4 k}{(2\pi)^4} A'(k^2 + x(1 - x)q^2), \\
&\int_C d\omega \rho(\omega) I(q^2, \omega) \omega = \\
&i \int_0^1 dx \int \frac{d^4 k}{(2\pi)^4} B'(k^2 + x(1 - x)q^2),
\end{aligned} \tag{B4}$$

and so on. The integrals can be evaluated by passing to the Euclidean space $k^2 \rightarrow -k_E^2$ and $(-i)d^4 k \rightarrow \pi^2 k_E^2 dk_E^2 = \pi^2 ds ds$. We may then shift the integration variable in order to get, *e.g.*,

$$\begin{aligned}
J(q^2) &= -i \int_0^1 dx \int \frac{d^4 k}{(2\pi)^4} F(k^2 + x(1 - x)q^2) \\
&= \frac{1}{16\pi^2} \int_0^\infty ds \int_0^1 dx F(-s + x(1 - x)q^2) \\
&= \frac{1}{16\pi^2} \int_0^\infty dS F(-S) \int_0^1 dx [S + x(1 - x)q^2]_+,
\end{aligned} \tag{B5}$$

where we have introduced the distribution $[x]_+ = x\theta(x)$. Let us assume that for definiteness $q^2 < 0$. Then, the argument of the step function vanishes for $x < x_-$ and $x > x_+$, where

$$x_{\pm} = \frac{1}{2} \pm \sqrt{1 + \frac{4S}{q^2}}. \tag{B6}$$

We have

$$\begin{aligned}
&\int_0^1 dx [S + x(1 - x)q^2]_+ = S + \frac{q^2}{6} \\
&- \theta(-q^2 - 4S) \sqrt{1 + \frac{4S}{q^2}} (q^2 + 4S).
\end{aligned} \tag{B7}$$

Thus

$$\begin{aligned}
J(q^2) &= -\frac{1}{16\pi^2} \left\{ \int_0^\infty dS F(-S) \left(S + \frac{q^2}{6} \right) \right. \\
&\quad \left. - \int_0^{-q^2/4} dS F(-S) \sqrt{1 + \frac{4S}{q^2}} (q^2 + 4S) \right\}.
\end{aligned} \tag{B8}$$

¹⁴ There is a typo in Eq. (A4) of Ref. [53].

This formula can be analytically continued to any complex q , and the second integral becomes a line integral in the complex S -plane. Clearly, if the function $F(-S)$ has a cut at say $S = -M_V^2/4$, the result of the line integral becomes path dependent and will develop an imaginary part discontinuity for $q^2 > M_V^2$. This is the way how a quark propagator with no poles generates the unitarity cuts in the two point correlators.

We list the final results:

$$\begin{aligned} \int_C d\omega \rho(\omega) I(q^2, \omega) &= \int_C d\omega \rho(\omega) I(0, \omega) \\ &+ \frac{1}{(4\pi)^2} \left[-\log \left(1 - \frac{q^2}{M_V^2} \right) + \frac{2}{3} \frac{q^2}{M_V^2 - q^2} \right], \\ \int_C d\omega \rho(\omega) I(q^2, \omega) \omega &= -\frac{\langle \bar{q}q \rangle}{2N_c} \frac{1}{M_S^2 - q^2}, \\ \int_C d\omega \rho(\omega) I(q^2, \omega) \omega^2 &= \frac{M_V^2}{96\pi^2} \frac{M_V^2}{M_V^2 - q^2}, \\ \int_C d\omega \rho(\omega) I(q^2, \omega) \omega^3 &= \\ -\frac{\langle \bar{q}q \rangle}{8N_c} \left[\frac{M_S^2}{M_S^2 - q^2} - 3 \frac{M_S}{q} \tanh^{-1} \frac{q}{M_S} \right]. \end{aligned} \quad (\text{B9})$$

APPENDIX C: QUANTUM-MECHANICAL EXAMPLES OF COMPLEX-MASS SYSTEMS

Establishing analytic properties of the Dirac operator eigenvalues for a complex mass is an involved mathematical problem. To gain some insight and develop some intuition, in this Appendix we consider a few cases of non-relativistic quantum mechanical system with complex coupling potentials. Our aim is to define what we mean by the *energy eigenvalues for a complex coupling*, assuming that we know the definition for the real coupling, and to determine its analytic properties in the complex plane. The most natural and obvious way to do so is in terms of analytic continuation in the coupling from the real case.

As a first example let us consider the harmonic oscillator which has the reduced potential $U = 2mV = m^2\omega^2x^2$ and the ground state energy is given by $E_0(\omega) = \omega/2$ for real $\omega > 0$. The problem is obviously invariant under the change $\omega \rightarrow -\omega$, and we should write $E_0(\omega) = |\omega|/2$ for real ω . Clearly, we have a branch cut at $\omega = 0$ as a function of the coupling ω^2 , hence the right way to write the energy for a complex coupling is $E_0(\omega) = \sqrt{\omega^2}/2$. Written this way the bound state wave function is given by $\psi_0 = Ce^{-\sqrt{\omega^2}x^2/2}$. The analytic continuation of the decreasing exponential becomes an increasing exponential on the second Riemann sheet, $\omega^2 \rightarrow e^{2\pi i}\omega^2$. For negative ω^2 we have a negative energy. So, the energies on the first and second Riemann sheets differ only in the sign.

As a second example let us consider the hydrogen atom where we have $V = -Z/r$ with $Z > 0$ and the energy

is $E_0(Z) = -Z^2/2$. This suggests an analytic behavior in Z , and in particular having a continued bound state solution for repulsive potentials ($Z < 0$). Again, the bound state function $u(r) = re^{-Zr}$ transforms into a positive exponential for negative Z . So, we have a cut at $Z = 0$. For negative Z we have a real energy but it is on the second Riemann sheet. In this case the energy on the first and the second Riemann sheets coincide.

As a final example, more directly related to the more complicated case of the toy model for the Dirac equation in Appendix D, we analyze the complex square well potential for which we have $U(r) = -U_0\Theta(R-r)$, with U_0 complex. For real U_0 the s-wave bound state solution is given by (we take $2m = 1$)

$$u(r) = \Theta(R-r)Ae^{-\kappa r} + \Theta(r-R)B \sin Kr \quad (\text{C1})$$

where

$$\kappa = \sqrt{-E}, \quad K = \sqrt{U_0 - E} \quad (\text{C2})$$

The continuity condition for the logarithmic derivative yields the bound state relation

$$-\kappa = K \cot KR \quad (\text{C3})$$

which defines an implicit function $E_0(U_0)$ which we want to extend to complex U_0 . For real U_0 there is a critical value $U_{0,c} = (\pi/2R)^2$ above which the equation has real solutions. Actually, close to the threshold we have for $U_0 > U_{0,c}$ the ground state

$$\begin{aligned} E_0(U_0) &= -\frac{1}{4}R^2(U_0 - U_{0,c})^2 \\ &+ \frac{1}{8}R^4 \left(1 - \frac{4}{\pi^2} \right) (U_0 - U_{0,c})^3 + \dots, \end{aligned} \quad (\text{C4})$$

which suggests an analytic behavior of the energy. Again, it is the wave function at large distances where we see that $\kappa \rightarrow -\kappa$ if we loop once about the critical point $U_{0,c} = (\pi/2R)^2$ in the complex U_0 plane. In this particular case, this corresponds to the well known fact that a square well potential with a subcritical coupling has a virtual state and no bound state. As $U_0 \rightarrow 0^+$ one gets $\kappa \rightarrow -\infty$ or $E_0 \rightarrow -\infty$ on the second Riemann sheet. Similar features should appear also for excited states, E_n , with the corresponding critical values. Thus, we may define the continuous function $E_0(U_0)$ for all real values of U_0 . For $U_0 > U_{0,c}$ it corresponds to a bound state, whereas for $U_0 < U_{0,c}$ it describes a virtual state.

If we go now to the complex plane in U_0 we get the implicit function defined through

$$A(k, U) = 0 \quad (\text{C5})$$

If we have a solution $A(k_0, U_0) = 0$ and go close to it, then by Taylor expanding we get

$$\begin{aligned} 0 &= A(k_0 + \Delta k, U_0 + \Delta U) \\ &= A(k_0, U_0) + \frac{\partial A(k_c, U_c)}{\partial k} \Delta k + \frac{\partial A(k_c, U_c)}{\partial U} \Delta U \end{aligned} \quad (\text{C6})$$

This way we can define a one to one relation unless either derivative vanishes at a critical point

$$\frac{\partial A(k_c, U_c)}{\partial k} = 0 \quad \text{or} \quad \frac{\partial A(k_c, U_c)}{\partial U} = 0 \quad (\text{C7})$$

If this is the case we have a square root branch point assuming

$$\frac{\partial^2 A(k_c, U_c)}{\partial k^2} \neq 0 \quad (\text{C8})$$

In our case we have the critical points located at

$$-\kappa = K \cot(KR) \quad (\text{C9})$$

$$-1 = \frac{\kappa R}{\sin(KR)^2} + \frac{\kappa}{K} \cot(KR) \quad (\text{C10})$$

Combining both equations we get

$$\kappa_c = -\frac{1}{R} \quad E_c = -\frac{1}{R^2} \quad (\text{C11})$$

$$1 = KR \cot(KR) \quad U_c = \frac{1 + x_n^2}{R^2} \quad (\text{C12})$$

with $x_n = 0, \pm 4.49, \pm 7.72, \pm 10.9, \dots$ Moreover, we have

$$\frac{\partial^2 A(k_c, U_c)}{\partial k^2} = \frac{R^3 U_c}{R^2 U_c - 1} \quad (\text{C13})$$

which diverges for $U_c = 1/R^2$. Note that the critical points are located in the second Riemann sheet. They generate branch points of second order, *i.e.* looping twice around the point the function returns to its original value. The Riemann surface is obtained by joining all critical points with a line. Since they are infinitely many, the cut divides the complex U plane into two disjoint pieces. The complete and extensive study of Riemann sheets of this particular problem can be looked up at Ref. [83].

The main outcome is that the analytic structure of a the analytically continued eigenvalues of a complex coupling potential can be determined by the study of the critical points which generate branch cuts. Otherwise, the function is analytic in the complex coupling plane. This situation appears also in Appendix D for the Dirac operator with a complex mass.

APPENDIX D: ANALYTIC PROPERTIES OF THE VALENCE EIGENSTATE IN A TOY MODEL

The discussion in Sect. III made explicit use of the fact that an integration path in the complex mass plane of the Dirac Hamiltonian can be deformed without pinching any singularities. Although we cannot prove this in general, the complex-mass coupling Dirac systems may have unusual properties. In this appendix we investigate a model bearing similarity to the full chiral model where our assumptions are verified. The main issue is both to define the meaning of an eigenvalue as a *function* of

the complex mass ω as well as to determine its analytic properties in the complex-mass plane. To our knowledge this topic is not discussed in the literature at all. However, strong similarities are found with the analytic properties of the energy eigenvalues of complex potentials, which have been motivated in the context of optical models [84, 85] and for review purposes Appendix C includes some warm-up quantum-mechanical problems which may be helpful in the understanding of analyticity properties that arise in studies of our type. The prescription for valenceness derived in Sect. III holds under specific conditions. In the chiral soliton model we have no precise knowledge of the analytic properties, hence it is not mathematically proven that the prescription can actually be used. The model of this section is much simpler and solvable semi-analytically. It shows that the desired analytic properties are fulfilled, providing support for the method in application to the chiral soliton model described in this paper.

Let us consider the Dirac equation for the state with 0 grand-spin and positive parity, $G^P = 0^+$, with the upper component u and the lower component v . It has the form

$$\begin{aligned} u' &= -uM \sin \theta - v(\epsilon + M \cos \theta) \\ v' &= u(\epsilon - M \cos \theta) + v(-\frac{2}{r} + M \sin \theta) \end{aligned} \quad (\text{D1})$$

with the usual boundary conditions for a normalizable state

$$u'(0) = 0, v(0) = 0, u(\infty) = 0, v(\infty) = 0. \quad (\text{D2})$$

Following Ref. [86] we look for a solution with the profile function

$$\theta(r) = \pi \Theta(R - r), \quad (\text{D3})$$

where $\Theta(x)$ the standard Heaviside step function. The profile (D3) has the winding number $(\theta(0) - \theta(\infty))/\pi = 1$. The analytic solution is

$$\begin{aligned} u(r) &= N \left(\Theta(R - r) \frac{\kappa^3}{\epsilon + M} \frac{\sinh \kappa r}{r} \right. \\ &\quad \left. + \Theta(r - R) \frac{\kappa^3}{M - \epsilon} \frac{e^{-\kappa r}}{r} \right), \\ v(r) &= N \left(\Theta(R - r) \frac{\kappa}{r^2} (\kappa r \cosh(\kappa r) - \sinh(\kappa r)) \right. \\ &\quad \left. + \Theta(r - R) \kappa (\kappa r + 1) \frac{e^{-\kappa r}}{r^2} \right), \end{aligned} \quad (\text{D4})$$

where $\kappa = \sqrt{M^2 - \epsilon^2}$ and N is the normalization factor chosen such that $N^2 \int d^3x (u^2 + v^2) = 1$. Using the matching condition expressing the continuity of $u(r)/v(r)$ at $r = R$ we get the eigenvalue equation

$$\kappa R \coth(\kappa R) = \frac{\kappa R(M - \epsilon) + 2M}{\epsilon + M} \quad (\text{D5})$$

which can be written in terms of dimensionless variables $x = \kappa R$ and $x_0 = MR$ as

$$x \coth(x) = \frac{x(x_0 \pm \sqrt{x_0^2 - x^2}) + 2x_0}{\pm \sqrt{x_0^2 - x^2} + x_0}, \quad (\text{D6})$$

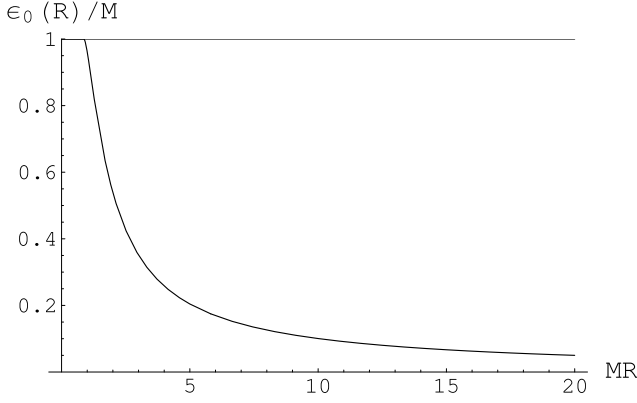


FIG. 9: Valence eigenvalue ϵ_0 for the toy model (D1,D3) as a function of the soliton size R in units of $1/M$.

where \pm corresponds to the positive (negative) energy states, $\epsilon > 0$ ($\epsilon < 0$). The value $x = 0$ is formally always a solution of Eq. (D6), but it does not correspond to a zero momentum state $\epsilon_0 = M$ since the solution is

$$u(r) = \frac{1}{R^2}\Theta(R-r) + \frac{2M}{r}\Theta(r-R) \quad (\text{D7})$$

$$v(r) = \Theta(R-r)\frac{2Mr}{3R^2} + \Theta(r-R)\frac{1}{r^2}, \quad (\text{D8})$$

which are regular both at $r = 0$ and $r = \infty$ but fail to fulfill the matching condition since $v/u = 2Mr/3$ for $r > R$ whereas $v/u = 2Mr$ for $r < R$.

The numerical dependence of the eigenvalue as a function of the soliton size for the 0^+ state in the toy model is depicted in Fig. 9. For large values of the soliton size at fixed mass we get

$$\epsilon_0(R) \rightarrow \frac{1}{R} \quad (\text{D9})$$

which means according to the scaling property that this behavior also holds true for large mass and fixed radius. The solution is always in the positive energy region and never dives into the sea (despite having topological number 1 – this was actually the point of Ref. [86]). For $R \rightarrow \infty$ one gets $\epsilon_0(R) \rightarrow 0^+$. The reason is related to the fact that always $\sin \theta = 0$ for the profile, and we have a scalar coupling for which $H\gamma_0\gamma_5 = -\gamma_0\gamma_5H$ and the spectrum is symmetric.

The threshold value for having a bound state is $(MR)^2 > 3/4$. Note that since $\kappa R = x$ changes sign across the threshold value, the bound state becomes virtual (exponentially growing). Thus, the analytic continuation of the unbound valence state for $R^2M^2 < 3/4$ is an exponentially growing state.

Equation (D6) defines implicitly a relation between x and x_0 . Actually, we can compute the inverse function

$$x_0^2 = \frac{x^4 (\coth(x) + 1)^2}{4(x+1)(x \coth(x) - 1)} \quad (\text{D10})$$

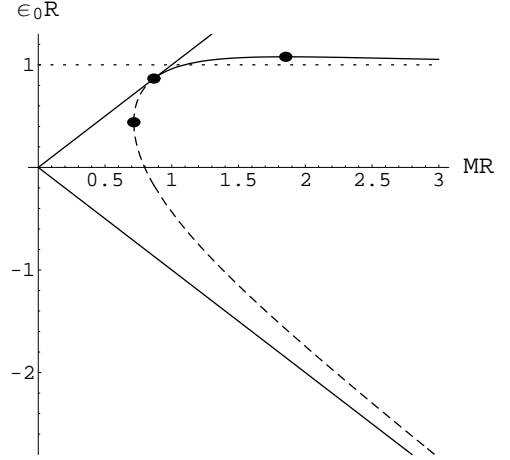


FIG. 10: Solid straight lines are $\epsilon = \pm M$, the solid curve is the bound state, the dashed curve is the virtual state. Blobs indicate the position of the saddle, the emergence of a bound state, and the bifurcation point of two real virtual states into two complex states. For the bound state $\epsilon_0 R$ approaches unity at $MR \rightarrow \infty$, while for the virtual branch it approaches the negative continuum.

For $x > 0$ the function on the r.h.s. is a monotonously increasing function and thus the inverse is uniquely defined. The minimum takes place at $x = 0$ and assumes the value of $3/4$. Hence there are no positive energy bound state solutions for $x_0^2 \leq 3/4$. For $x_0^2 = 3/4$ we have a negative energy solution $\kappa R = x \simeq -0.848$ and $\epsilon \simeq -0.175/R$, of no concern here. For $0.512 \leq x_0^2 \leq 3/4$ we have a positive energy state with $\kappa < 0$. For $0.512 > x_0^2$ the value of κ becomes complex. For $x_0 \rightarrow 0$ we get $x \rightarrow -\infty$.

In summary, for the real-mass case we have

- For $0.866 < x_0$ we have one bound state solution.
- For $0.797 < x_0 < 0.866$ we have one virtual state solution.
- For $0.712 < x_0 < 0.797$ we have two virtual states. For $x_0 = 0.7968$ one at $x = -0.797$ and the other one at $x = -0.196$, the higher one being a continuation of the previous case.
- For $x_0 < 0.716$ the two solutions collide at $x = -0.574$ and bifurcate into the complex plane.

So clearly for $x_0 < 0.797$ we have a cut in the κ plane. The situation for the real mass case has been displayed in Fig. 10. This plot should be compared with the exponential soliton profile of Fig. 2.

We can now proceed to the complex plane in ω . The obvious way to define the eigenvalue $\epsilon_0(\omega)$ as a function of the complex variable ω is by analytic continuation, since we want to follow the evolution of the state in the complex-mass plane. For illustration purposes we plot in Fig. 11 the corresponding analytically continued eigenvalues when $\omega = e^{i\alpha}$ for several soliton sizes R .

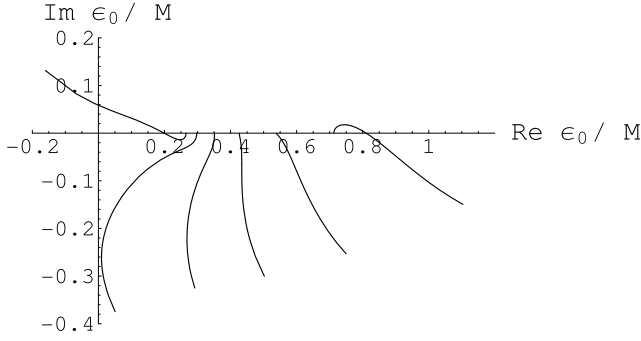


FIG. 11: analytically continued complex valence eigenvalue $\epsilon_0(R, \omega)$ in the toy model plotted as a function of the complex mass $\omega = e^{i\alpha}$ for α in the first quadrant, $0 \leq \alpha \leq \pi/2$. The axes represent $\text{Re}(\epsilon_0)$ and $\text{Im}(\epsilon_0)$. Subsequent curves, from right to left, correspond to increasing values of $R = 2, 2.5, 3, 3.5, 3.9$. The points on the real axis are for $\alpha = 0$, and the value of α parameterizes the curves, which evolve away from the real axis. The other quadrants are obtained by reflection about the real axis.

Equivalently, we consider the function of the variable x_0^2 . Thus, we take the solutions which were defined for real M fulfilling the boundary conditions and arrive at the transcendental equation (D6), which now defines implicitly $\epsilon_0(\omega)$.¹⁵ Thus, if we differentiate with respect to x the implicit function we get the equation for the critical points

$$\frac{2t^4 + t^3 - 4t^2 - 2t + 1 + (2t + 3)\sqrt{1 - t^2}}{t\sqrt{1 - t^2}(1 + \sqrt{1 - t^2})^2} = 0, \quad (\text{D11})$$

where for simplicity the variable $t = x/x_0$ has been introduced. This is an algebraic equation with solutions $t = t_n$. We find numerically

$$t_n = x/x_0 = -1.2741 \pm i0.1174, 0.9092, 1.3898 \pm i0.4832, \dots, \quad (\text{D12})$$

which forms a bundle of solutions

$$t_n x_0 \coth(t_n x_0) = \frac{x_0 t_n (1 - \sqrt{1 - t_n^2}) + 2t_n}{\sqrt{1 - t_n^2} + 1}. \quad (\text{D13})$$

We see that for any value of t_n there are infinitely many solutions for x_0 . Roughly, they are located along a straight line. For instance, for $x/x_0 = 0.9092$ the critical points in x_0 are located at about $x_0 = 0.5 + i n \pi$ for large- N . So, the whole critical points structure looks like five straight lines running in all directions. An alternative technique to analyze this kind of problems is by using

¹⁵ According to the implicit function theorem the equation $y = f(x)$ can be inverted around the solution $y_0 = f(x_0)$ if $f'(x_0) \neq 0$. Critical points for which $f'(x_0) = 0$ define bifurcation branches if $f''(x_0) \neq 0$.

the modular landscape of the exponential as explained in detail in Refs. [84, 85].

The upshot of this study is that $\epsilon(\omega)$ has only critical points on the second Riemann sheet. This means that whenever the bound state becomes unbound we are crossing the branch cut, which happens for sufficiently small values of ω . For the spectral integral that would set the condition $M_c < M_V/2$ not to have cut intersection between the spectral function and the energy function.¹⁶

APPENDIX E: COMPUTING THE SPECTRAL INTEGRAL FOR THE VALENCE CONTRIBUTION FIRST

In this appendix we show how our basic result for the valence contribution, Eq. (86), can be reproduced by evaluating the spectral integral first. In fact, experience with perturbative calculations of quantities such as f_π or the pion form factor suggest that there is no danger in computing the ω integral first. At finite temperature this is actually the only way to get analytic results [88]. To compute the troublesome spectral integral first in the soliton case, we transform the scalar-pseudoscalar coupling into a vector-axial derivative coupling and a constant mass. We write

$$(i\partial - \omega U^5) = u^5 (i\partial + u^{-5} i\partial u^{-5} - \omega) u^5 \quad (\text{E1})$$

where $u^2 = U$. This is a field dependent axial rotation and at the level of the determinant of the Dirac operator generates the anomalous Wess-Zumino term in the SU(3) case. Then, we get

$$\begin{aligned} S_{aa'}(x, x') &= \int d\omega \rho(\omega) \\ &\times \langle x | \left[u^{-5} (i\partial + u^{-5} i\partial u^{-5} - \omega)^{-1} u^{-5} \right]_{aa'} | x' \rangle \\ &= \left[\langle x | u^{-5} \left\{ \int d\omega \frac{\rho(\omega)}{i\partial + u^{-5} i\partial u^{-5} - \omega} \right\} u^{-5} | x' \rangle \right]_{a,a'} \\ &= [u(x)^{-5} \langle x | S (i\partial + u^{-5} i\partial u^{-5}) | x' \rangle u(x')^{-5}]_{a,a'}. \end{aligned} \quad (\text{E2})$$

Now, in the meson dominance model the propagator function is given by

$$S(p) = \int_C d\omega \frac{\rho(\omega)}{p - \omega} = 2\pi i \rho(p) + \frac{1}{p}. \quad (\text{E3})$$

This relation is obtained for the closed contour under the assumption that $\rho(\omega)$ has a pole only at $\omega = 0$, which

¹⁶ Obviously, the smaller M_c the better. Now, it would be interesting to see if there are chiral angles $\theta(r)$ for which one always has a bound state. In such a case cuts would not intersect. This is not such a strange situation, since e.g. in one dimensional quantum mechanics, any tiny attractive potential generates immediately a bound state. Also, in 1+1 dimensions the chiral angle $\theta(x) = \alpha \text{sign}(x)$ has always a bound state $\epsilon = M \cos(\alpha)$ [87].

is clearly the case of the meson dominance model (20). Equation (E3) is just a functional relation, and does not depend on the fact that the variable \not{p} is a matrix. We have indeed computed the spectral integral, but for this formula to be of any use, we have to look for the eigenvalue problem of the chirally rotated Dirac operator

$$(i\cancel{\partial} + u^{-5}i\cancel{\partial}u^{-5}) \Phi_n = M_n \Phi_n. \quad (\text{E4})$$

This eigenvalue problem may be tricky in practice since the operator is not normal, *i.e.* the adjoint operator does not commute with the original operator even if we go to the Euclidean space (where the derivative and the vector part of the coupling are anti self-adjoint and the axial part is self adjoint). This means that M_n may be complex in general.

Undoing field dependent chiral rotation we get

$$(i\cancel{\partial} - M_n U^5) \Psi_n = 0, \quad (\text{E5})$$

where

$$\Psi_n = u^{-5} \Phi_n, \quad \Psi_n^\dagger = \Phi_n^\dagger u^{-5}. \quad (\text{E6})$$

Thus, the eigenvalue problem corresponds to the search for the (eigen)masses of the original Dirac operator which yield a zero mode of the four dimensional Dirac operator. This equation looks as an on-shell condition for the bound quarks. In the stationary field case we have, $\Psi_n(\vec{x}, t) = e^{-i\epsilon t} \psi_n(\vec{x})$. At this point we must make a choice on the values of ϵ . A natural condition would be to request an exponential damping in the Euclidean space. Thus, we take ϵ real and positive for forward propagating states, $t > 0$, and negative for backward propagating states. (Another possibility that would be to take a contour with conditions on $\text{Re } \epsilon$),

$$[-i\alpha \cdot \nabla + M_n \beta U^5] \psi_n = \epsilon \psi_n. \quad (\text{E7})$$

Thus, here we encounter just the opposite problem to the case of the spectral mass problem; for a given energy we have to look for the eigenmasses, $M_n(\epsilon)$ (instead of $\epsilon_n(\omega)$). Actually, this looks like an isospectral problem; given the energy how many chiral couplings possess the same energy. Thus, the eigenvectors of this problem are not exactly the eigenvectors of the standard Dirac Hamiltonian problem. Note also that because we are searching for zero modes of the Dirac operator its eigenvectors are also eigenvectors of the Dirac Hamiltonian, which is not the case for non-zero eigenvalues, *i.e.* $\gamma_0(i\partial_t - H)\Psi_n = \lambda_n \Psi_n$ with $\lambda_n \neq 0$ cannot be solved by a eigenstate of H because of the γ_0 . Clearly, multivaluedness issues may become quite relevant when discussing the possible equivalence of both problems. On the other hand, $H^\dagger = H$ if and only if $M_n(\epsilon)$ is real. For such a case if both M_n and ϵ are real, then bound states happen for $-M_n < \epsilon < M_n$. In general M_n is complex, since even in the free case, $U = 1$, we have $M_n(\epsilon) = \sqrt{\epsilon^2 - k_n^2}$, with k_n denoting the momentum quantized due to box

boundary conditions. Then, we are lead to

$$\begin{aligned} S_{aa'}(x, x') &= u^{-5}(x) \langle x | S(i\cancel{\partial} + u^{-5}i\cancel{\partial}u^{-5}) | x' \rangle u^{-5}(x') \\ &= u^{-5}(x) \sum_n \Phi_n(x) S(M_n) \Phi_n^\dagger(x') u^{-5}(x') \\ &= \sum_n \Psi_n(x) S(M_n) \Psi_n^\dagger(x') \\ &= \int_{-\infty}^{\infty} \frac{d\epsilon}{2\pi} \sum_n \psi_n(x) \left[e^{i\epsilon(t-t')} \theta(\epsilon) \theta(t' - t) \right. \\ &\quad \left. + e^{-i\epsilon(t-t')} \theta(-\epsilon) \theta(t - t') \right] S(M_n(\epsilon)) \psi_n^\dagger(x'). \end{aligned} \quad (\text{E8})$$

In this representation, the states propagating forward in time have been chosen to be those of positive energy and we are led to the basic integral

$$\int_0^\infty \frac{d\epsilon}{2\pi} e^{-\tau\epsilon} S(M_n(\epsilon)) = \int_0^\infty \frac{d\epsilon}{2\pi} e^{-\tau\epsilon + \log S(M_n(\epsilon))}, \quad (\text{E9})$$

with $\tau \rightarrow \infty$. The function $S(M)$ of Eq. (E3) has no poles but branch cuts starting at $M = \pm M_V/2$. The stationary points are determined from the equation

$$\tau = \frac{\partial \log S(M_n(\epsilon))}{\partial \epsilon} = M'_n(\epsilon) \frac{S'(M_n(\epsilon))}{S(M_n(\epsilon))}. \quad (\text{E10})$$

Note that a real $S(M)$ requires $M_n < M_V/2$, thus for $M_n(\epsilon) \neq M_V/2$ we must have a divergent $M'_n(\epsilon) \rightarrow \pm\infty$. Obviously, the smallest positive ϵ (the valence orbit) fulfilling $1/M'_n(\epsilon) = 0$ dominates, and we get the relation

$$\epsilon_0 = \min \epsilon \Big|_{M'_n(\epsilon)=\infty, \epsilon>0}, \quad (\text{E11})$$

in agreement with our result of Sect. (III), which is the result equivalent to (84) written in terms of the inverse function.

APPENDIX F: EVALUATION OF THE DIRAC SEA CONTRIBUTION TO SOLITON OBSERVABLES

Dirac sea contributions to observables involve the complex mass integral. However, it is possible to rewrite this contribution as a real mass distribution. The vector spectral density ρ_V can be written as

$$\rho_V(\omega) = \frac{d^2}{du^2} \bar{\rho}_V(\omega) \Big|_{u=1/M_V^2}, \quad (\text{F1})$$

where

$$\bar{\rho}_V(\omega) = \frac{1}{2\pi i} \frac{1}{12\omega^5} \frac{1}{(1 - 4u\omega^2)^{1/2}}. \quad (\text{F2})$$

The function $\bar{\rho}_V(\omega)$ has the property that its integrals with smooth functions vanish along the parts of the contour C encircling the branch points of Fig. 1, as well as

are finite along the cut. Similarly, for the scalar part, ρ_S , we have

$$\rho_S(\omega) = \frac{d^2}{du^2} \bar{\rho}_S(\omega) \Big|_{u=1/M_V^2}, \quad (\text{F3})$$

with

$$\bar{\rho}_S(\omega) = \frac{1}{2\pi i} \frac{1}{12\omega^4} \frac{12\rho'_3}{M_S^4(1-4u\omega^2)^{1/2}}. \quad (\text{F4})$$

We now define

$$\begin{aligned} \bar{A}_{\text{sea},V}(u) &= 2 \int_{1/(2\sqrt{u})}^{\infty} d\omega \text{disc}[\bar{\rho}_V(\omega)] \frac{A_{\text{sea}}(\omega) + A_{\text{sea}}(-\omega)}{2}, \\ \text{disc}[\bar{\rho}_V(\omega)] &= \frac{1}{12\pi\omega^5 \sqrt{4u\omega^2 - 1}}, \end{aligned} \quad (\text{F5})$$

(the factor of 2 comes from the two sections of C) and, similarly,

$$\begin{aligned} \bar{A}_{\text{sea},S}(u) &= 2 \int_{1/(2\sqrt{u})}^{\infty} d\omega \text{disc}[\bar{\rho}_S(\omega)] \frac{A_{\text{sea}}(\omega) - A_{\text{sea}}(-\omega)}{2}, \\ \text{disc}[\bar{\rho}_S(\omega)] &= \frac{\rho'_3}{\pi M_S^4 \omega^4 \sqrt{4u\omega^2 - 1}}. \end{aligned} \quad (\text{F6})$$

The Dirac-sea contributions to observables are now obtained from

$$A_{\text{sea}} = \frac{d^2}{du^2} [\bar{A}_{\text{sea},V}(u) + \bar{A}_{\text{sea},S}(u)] \Big|_{u=1/M_V^2}. \quad (\text{F7})$$

Thus, we have managed to “put the model on the real axis”, at the only expense of the need of differentiation with respect to u at the end of the calculation. As a bonus we also get a very high degree of convergence at large ω , since $\text{disc}[\bar{\rho}_V(\omega)] \sim 1/\omega^6$ and $\text{disc}[\bar{\rho}_S(\omega)] \sim 1/\omega^5$. It is useful to get rid of the integrable singularities in Eqs. (F5,F6) by means of introducing the variable

$$z = \sqrt{4u\omega^2 - 1}, \quad \omega = \frac{\sqrt{z^2 + 1}}{2\sqrt{u}}. \quad (\text{F8})$$

Then

$$\begin{aligned} \bar{A}_{\text{sea},V}(u) &= \frac{8u^2}{3\pi} \int_0^{\infty} \frac{dz}{(z^2 + 1)^3} \\ &\times \frac{1}{2} \left[A_{\text{sea}} \left(\frac{\sqrt{z^2 + 1}}{2\sqrt{u}} \right) + A_{\text{sea}} \left(-\frac{\sqrt{z^2 + 1}}{2\sqrt{u}} \right) \right], \end{aligned} \quad (\text{F9})$$

and

$$\begin{aligned} \bar{A}_{\text{sea},S}(u) &= -\frac{8\pi \langle \bar{q}q \rangle}{N_c M_V^4} (4u)^{3/2} \int_0^{\infty} \frac{dz}{(z^2 + 1)^{5/2}} \\ &\times \frac{1}{2} \left[A_{\text{sea}} \left(\frac{\sqrt{z^2 + 1}}{2\sqrt{u}} \right) - A_{\text{sea}} \left(-\frac{\sqrt{z^2 + 1}}{2\sqrt{u}} \right) \right]. \end{aligned} \quad (\text{F10})$$

The Dirac Hamiltonian has the form

$$H(\omega, m) = -i\alpha \cdot \nabla + \beta m + \beta \omega U^5, \quad (\text{F11})$$

with the corresponding Dirac equation

$$H(\omega, m)|i; \omega, m\rangle = \epsilon_i(\omega, m)|i; \omega, m\rangle. \quad (\text{F12})$$

It has the property

$$\begin{aligned} \gamma_5 H(\omega, m) \gamma_5 &= H(-\omega, -m), \\ \gamma_5 |i; \omega, m\rangle &= |i; -\omega, -m\rangle. \end{aligned} \quad (\text{F13})$$

Thus γ_5 flips the sign of the current quark mass m and ω . Obviously, the spectrum of the operator is unchanged under this similarity transformation. Nevertheless, it is convenient in the numerical work to deal with positive values of ω only. Thus, any one body observable at negative ω can be transformed according to

$$\begin{aligned} A_{\text{sea}}(\omega) &= \sum_i \langle i; \omega, m | a(\omega, m) | i; \omega, m \rangle \\ &= \sum_i \langle i; \omega, m | \gamma_5 a(\omega, m) \gamma_5 | i; \omega, m \rangle \\ &= \sum_i \langle i; -\omega, -m | \gamma_5 a(\omega, m) \gamma_5 | i; -\omega, -m \rangle. \end{aligned} \quad (\text{F14})$$

Some examples of $\gamma_5 a(\omega, m) \gamma_5$ encountered in the evaluation of observables are $\gamma_5 H(\omega, m) \gamma_5 = H(-\omega, -m)$, $\gamma_5 \beta \gamma_5 = -\beta$, *etc.* The formula for the energy following from the above formulation is given in Eq. (106,107).

APPENDIX G: INSTABILITY OF THE LINEAR MODEL

Although SQM is only constructed in the nonlinear case, it looks tempting to extend it in the spirit of the original bosonized NJL model to a linear version where the fields may depart from the chiral circle,

$$\begin{aligned} I &= i \int_C d\omega \rho(\omega) \text{Tr} \log(i\bar{\phi} - m - w(s + i\gamma_5 \boldsymbol{\tau} \cdot \mathbf{p})) \\ &+ \frac{1}{2g^2} \int d^4x (s^2 + \mathbf{p}^2). \end{aligned} \quad (\text{G1})$$

Here s and \mathbf{p} denote the scalar-isoscalar and pseudoscalar-isovector fields, and g is a coupling constant. The meson fields s and p are dimensionless. In the chiral limit and in the vacuum ($s = 1$, $p = 0$) we find from the Euler-Lagrange equation for the s field the condition

$$\begin{aligned} \frac{s}{g^2} &= -i \int_C d\omega \rho(\omega) \text{Tr} \frac{\omega}{i\bar{\phi} - \omega s} \\ &= -4i N_c N_f \int_C d\omega \rho(\omega) \int \frac{d^4k}{(2\pi)^4} \frac{\omega^2 s}{k^2 - (\omega s)^2}. \end{aligned} \quad (\text{G2})$$

With the explicit form of the meson-dominance spectral function (20) and the techniques of Ref. [53] we find

$$\frac{1}{g^2} = \frac{N_c N_f M_V^4}{48\pi^2}. \quad (\text{G3})$$

The effective potential assumes the form

$$V = \frac{I}{\int d^4x} = \frac{N_c N_f M_V^4}{192\pi^2} (2s^2 - s^4), \quad (\text{G4})$$

where the s^4 term originates from the first term in Eq. (G1). This corresponds to an inverted Mexican Hat, and clearly displays instability. Therefore the linear version of the model (G1) does not make sense.

It is worthwhile to mention that this feature should

not be regarded as specific to the spectral regularization. The inverted potential also arises when renormalizing the fermion determinant with the help of the ζ -function regularization in the local NJL model. Therefore one needs to use from the outset the non-linear realization of chiral symmetry on its own, and it cannot be treated as an approximation to the linear model. In that regard we also note that the soliton instability in linear NJL models has been found in Ref. [89].

-
- [1] T. H. R. Skyrme, Proc. Roy. Soc. Lond. **A260**, 127 (1961).
 - [2] G. 't Hooft, Nucl. Phys. **B72**, 461 (1974).
 - [3] E. Witten, Nucl. Phys. **B160**, 57 (1979).
 - [4] J. Goldstone and F. Wilczek, Phys. Rev. Lett. **47**, 986 (1981).
 - [5] E. Witten, Nucl. Phys. **B223**, 422 (1983).
 - [6] A. P. Balachandran, V. P. Nair, S. G. Rajeev, and A. Stern, Phys. Rev. **D27**, 1153 (1983).
 - [7] G. S. Adkins, C. R. Nappi, and E. Witten, Nucl. Phys. **B228**, 552 (1983).
 - [8] G. Holzwarth and B. Schwesinger, Rept. Prog. Phys. **49**, 825 (1986).
 - [9] I. Zahed and G. E. Brown, Phys. Rept. **142**, 1 (1986).
 - [10] H. Weigel, Int. J. Mod. Phys. **A11**, 2419 (1996).
 - [11] J. Schechter and H. Weigel (1999), hep-ph/9907554.
 - [12] H. Weigel, Eur. Phys. J. **A21**, 133 (2004).
 - [13] M. Chemtob, Nucl. Phys. **A473**, 613 (1987).
 - [14] M. C. Birse and M. K. Banerjee, Phys. Lett. **B136**, 284 (1984).
 - [15] M. C. Birse and M. K. Banerjee, Phys. Rev. **D31**, 118 (1985).
 - [16] S. Kahana, G. Ripka, and V. Soni, Nucl. Phys. **A415**, 351 (1984).
 - [17] G. Kaelbermann and J. M. Eisenberg, Phys. Lett. **B139**, 337 (1984).
 - [18] W. Broniowski and M. K. Banerjee, Phys. Lett. **B158**, 335 (1985).
 - [19] W. Broniowski and M. K. Banerjee, Phys. Rev. **D34**, 849 (1986).
 - [20] D. Diakonov, V. Y. Petrov, and P. V. Pobylitsa, Nucl. Phys. **B306**, 809 (1988).
 - [21] T. Meissner, E. Ruiz Arriola, F. Grummer, H. Mavromatis, and K. Goeke, Phys. Lett. **B214**, 312 (1988).
 - [22] M. Wakamatsu and H. Yoshiki, Nucl. Phys. **A524**, 561 (1991).
 - [23] H. Weigel, E. Ruiz Arriola, and L. P. Gamberg, Nucl. Phys. **B560**, 383 (1999).
 - [24] M. C. Birse, Prog. Part. Nucl. Phys. **25**, 1 (1990).
 - [25] D. Diakonov, Prog. Part. Nucl. Phys. **36**, 1 (1996).
 - [26] C. V. Christov, A. Blotz, H.-C. Kim, P. V. Pobylitsa, T. Watabe, Th. Meissner, E. Ruiz Arriola, and K. Goeke, Prog. Part. Nucl. Phys. **37**, 1 (1996).
 - [27] R. Alkofer, H. Reinhardt, and H. Weigel, Phys. Rep. **265**, 139 (1996).
 - [28] G. Ripka, *Quarks Bound by Chiral Fields* (Clarendon Press, Oxford, 1997).
 - [29] D. I. Diakonov and V. Y. Petrov, Nucl. Phys. **B 272**, 457 (1986).
 - [30] C. D. Roberts and A. G. Williams, Prog. Part. and Nucl. Phys. **33**, 475 (1994).
 - [31] R. D. Ball, Int. Journ. Mod. Phys. **A 5**, 4391 (1990).
 - [32] G. Ripka, *Quarks Bound by Chiral Fields* (Oxford University Press, Oxford, 1997).
 - [33] J. Praschifka, C. D. Roberts, and R. T. Cahill, Phys. Rev. **D 36**, 209 (1987).
 - [34] B. Holdom, J. Terning, and K. Verbeek, Phys. Lett. **B 232**, 351 (1989).
 - [35] M. Buballa and S. Krewald, Phys. Lett. **B 294**, 19 (1992).
 - [36] R. D. Ball and G. Ripka, in *Many Body Physics (Coimbra 1993)*, edited by C. Fiolhais, M. Fiolhais, C. Sousa, and J. N. Urbano (World Scientific, Singapore, 1993).
 - [37] R. D. Bowler and M. C. Birse, Nucl. Phys. **A582**, 655 (1995).
 - [38] R. S. Plant and M. C. Birse, Nucl. Phys. **A628**, 607 (1998).
 - [39] W. Broniowski, in *Hadron Physics: Effective theories of low-energy QCD, Coimbra, Portugal, September 1999, AIP Conference Proceedings*, edited by A. H. Blin, B. Hiller, M. C. Ruivo, C. A. Sousa, and E. van Beveren (AIP, Melville, New York, 1999), vol. 508, p. 380, nucl-th/9910057.
 - [40] W. Broniowski, Tech. Rep. 1828/PH, INP Cracow (1999), hep-ph/9909438, talk presented at the Mini-Workshop on *Hadrons as Solitons*, Bled, Slovenia, 6-17 July 1999.
 - [41] E. Ruiz Arriola and L. L. Salcedo, Phys. Lett. **B450**, 225 (1999).
 - [42] E. Ruiz Arriola and L. L. Salcedo, in *Hadron Physics: Effective theories of low-energy QCD, Coimbra, Portugal, September 1999, AIP Conference Proceedings*, edited by A. H. Blin, B. Hiller, M. C. Ruivo, C. A. Sousa, and E. van Beveren (AIP, Melville, New York, 1999), vol. 508, nucl-th/9910230.
 - [43] R. S. Plant and M. C. Birse (2000), hep-ph/0007340.
 - [44] D. Diakonov and V. Y. Petrov (2000), hep-ph/0009006.
 - [45] C. Gocke, D. Blaschke, A. Khalatyan, and H. Grigorian (2001), hep-ph/0104183.
 - [46] M. Praszalowicz and A. Rostworowski (2001), hep-ph/0105188.
 - [47] A. E. Dorokhov and W. Broniowski, Eur. Phys. J. **C32**, 79 (2003).
 - [48] B. Golli, W. Broniowski, and G. Ripka, Phys. Lett. **B437**, 24 (1998).
 - [49] W. Broniowski, B. Golli, and G. Ripka, Nucl. Phys. **A703**, 667 (2002).
 - [50] M. Praszalowicz, A. Blotz, and K. Goeke, Phys. Lett.

- B354**, 415 (1995).
- [51] W. Broniowski and T. D. Cohen, Nucl. Phys. **A458**, 652 (1986).
 - [52] E. Ruiz Arriola (2001), talk at *Workshop on Lepton Scattering, Hadrons and QCD*, Adelaide, Australia, 26 Mar - 6 Apr 2001, hep-ph/0107087.
 - [53] E. Ruiz Arriola and W. Broniowski, Phys. Rev. **D67**, 074021 (2003).
 - [54] E. Ruiz Arriola and W. Broniowski (2003), presented at *Light-Cone Workshop: Hadrons and Beyond (LC 03)*, Durham, England, 5-9 Aug 2003, hep-ph/0310044.
 - [55] E. Megias, E. Ruiz Arriola, L. L. Salcedo, and W. Broniowski, Phys. Rev. **D70**, 034031 (2004).
 - [56] G. V. Efimov and M. A. Ivanov, *The Quark confinement model of hadrons* (IOP, Bristol, UK, 1993).
 - [57] T. D. Lee and G. C. Wick, Nucl. Phys. **B9**, 209 (1969).
 - [58] R. E. Cutkosky, P. V. Landshoff, D. I. Olive, and J. C. Polkinghorne, Nucl. Phys. **B12**, 281 (1969).
 - [59] N. Nakanishi, Prog. Theor. Phys. Suppl. **51**, 1 (1972).
 - [60] V. N. Gribov, *Gauge Theories and Quark Confinement* (Phasis, Moscow, 2002).
 - [61] F. Kleefeld (2004), hep-th/0408028.
 - [62] E. Ruiz Arriola, Acta Phys. Pol. **B33**, 4443 (2002).
 - [63] R. Delbourgo and P. C. West, J. Phys. **A10**, 1049 (1977).
 - [64] R. Delbourgo, Nuovo Cim. **A49**, 484 (1979).
 - [65] A. E. Dorokhov, W. Broniowski and E. Ruiz Arriola, Phys. Rev. D **74**, 054023 (2006).
 - [66] W. Broniowski and E. Ruiz Arriola, Phys. Lett. **B649**, 49, 2007.
 - [67] W. Broniowski and E. Ruiz Arriola, Phys. Lett. **B574**, 57 (2003).
 - [68] P. O. Bowman, U. M. Heller, and A. G. Williams, Phys. Rev. **D66**, 014505 (2002).
 - [69] W. Broniowski, G. Ripka, E. Nikolov, and K. Goeke, Z. Phys. **A354**, 421 (1996).
 - [70] E. Ruiz Arriola and W. Broniowski, to appear in proc. *4th International Conference on Quarks and Nuclear Physics (QNP06)*, Madrid, 5-10 Jun 2006, hep-ph/0609266.
 - [71] E. Ruiz Arriola and W. Broniowski, Phys. Rev. D **73**, 097502 (2006).
 - [72] G. Ecker, J. Gasser, A. Pich, and E. de Rafael, Nucl. Phys. **B321**, 311 (1989).
 - [73] A. Pich (2002), proc. *The Phenomenology of Large N_c QCD*, Tempe, Arizona, 9-11 Jan 2002, ed. R. Lebed, World Scientific, Singapore, 2002, hep-ph/0205030.
 - [74] L. L. Salcedo and E. Ruiz Arriola, Ann. Phys. **250**, 1 (1996).
 - [75] D. Diakonov, V. Y. Petrov, and M. Praszalowicz, Nucl. Phys. **B323**, 53 (1989).
 - [76] I. Adjali, I. J. R. Aitchison, and J. A. Zuk, Nucl. Phys. **A537**, 457 (1992).
 - [77] G. Ripka and S. Kahana, Phys. Rev. **D36**, 1233 (1987).
 - [78] V. Soni, Phys. Lett. **B195**, 569 (1987).
 - [79] T. D. Cohen and W. Broniowski, Phys. Rev. **D34**, 3472 (1986).
 - [80] B. Golli and M. Rosina, Phys. Lett. **B165**, 347 (1985).
 - [81] M. C. Birse, Phys. Rev. **D33**, 1934 (1986).
 - [82] J. Gasser, H. Leutwyler, and M. E. Sainio, Phys. Lett. **B253**, 252 (1991).
 - [83] C. Grama, N. Grama, and I. Zamfirescu, Phys. Rev. **A61**, 032716 (2000).
 - [84] L. P. Kok and H. van Haeringen, Ann. Phys. **131**, 426 (1981).
 - [85] A. M. Badalian, L. P. Kok, M. I. Polikarpov, and Y. A. Simonov, Phys. Rept. **82**, 31 (1982).
 - [86] M.-s. Zhao and J. R. Hiller, Phys. Rev. **D40**, 1329 (1989).
 - [87] R. MacKenzie and F. Wilczek, Phys. Rev. **D30**, 2194 (1984).
 - [88] E. Megias, E. Ruiz Arriola, and L. L. Salcedo, Phys. Rev. **D74**, 065005 (2006).
 - [89] P. Sieber, T. Meissner, F. Gruemmer, and K. Goke, Nucl. Phys. **A547**, 459 (1992).